

**OFFICE OF CIVILIAN RADIOACTIVE WASTE MANAGEMENT
ANALYSIS/MODEL COVER SHEET**

1. QA: QA

Complete Only Applicable Items

Page: 1 of 70

2. **Analysis** Check all that apply

| | |
|--------------------------|--|
| Type of Analysis | <input type="checkbox"/> Engineering <input type="checkbox"/> Performance Assessment <input type="checkbox"/> Scientific |
| Intended Use of Analysis | <input type="checkbox"/> Input to Calculation <input type="checkbox"/> Input to another Analysis or Model <input type="checkbox"/> Input to Technical Document |
| Describe use: | |
| | |
| | |

3. **Model** Check all that apply

| | |
|-----------------------|--|
| Type of Model | <input type="checkbox"/> Conceptual Model <input type="checkbox"/> Mathematical Model <input checked="" type="checkbox"/> Process Model <input type="checkbox"/> Abstraction Model <input type="checkbox"/> System Model |
| Intended Use of Model | <input type="checkbox"/> Input to Calculation <input checked="" type="checkbox"/> Input to another Model or Analysis <input type="checkbox"/> Input to Technical Document |
| Describe use: | |
| Input to WAPDEG | |
| | |
| | |

4. Title:
General Corrosion and Localized Corrosion of the Drip Shield

5. Document Identifier (including Rev. No. and Change No., if applicable):
ANL-EBS-MD-000004 REV 00

6. Total Attachments:
N/A

7. Attachment Numbers - No. of Pages in Each:
N/A

| | Printed Name | Signature | Date |
|-------------------------|-----------------------------------|--------------------|---------|
| 8. Originator | Joseph Farmer, R. Daniel McCright | <i>[Signature]</i> | 3/20/00 |
| 9. Checker | Denny Jones | <i>[Signature]</i> | 3/21/00 |
| 10. Lead/Supervisor | Al Lingenfelter | <i>[Signature]</i> | 3/20/00 |
| 11. Responsible Manager | David Stahl | <i>[Signature]</i> | 3/21/00 |

12. Remarks:
The designated originator and lead author of this AMR is Joseph Farmer. Contributing authors and researchers include Venkataraman Pasupathi, Daniel McCright, Joann Horn, Tiengan Lan, Peter Bedrossian, Francis Wang, John Eastli, Ken King, Steve Gordon, Larry Logotetz, Beverly Lum and David Fiz. Technical comments by Joon Lee, Kevin Man and members of the NWTRB are gratefully acknowledged. Data tracking was coordinated by Michael Coatsworth and Tom Gibson, and the lead editor was Kim Hennmann. QA comments by Charlie Warren and Richard Powe are appreciated. Direct management and oversight included George Dial, Dan Wilkins, Jean Younker, Mike Lugo, Hugh Benton, David Stahl, Martha Kohler, and Al Lingenfelter. Work was sponsored by the U.S. Department of Energy Office of Civilian and Radioactive Waste Management (OCRWM). This work was done under the auspices of the U.S. Department of Energy (DOE) by Lawrence Livermore National Laboratory (LLNL) under Contract No. W-7405-Eng-48.

**OFFICE OF CIVILIAN RADIOACTIVE WASTE MANAGEMENT
ANALYSIS/MODEL REVISION RECORD**

Complete Only Applicable Items

1. Page: 2 of 70

2. Analysis or Model Title:

General Corrosion and Localized Corrosion of the Drip Shield

3. Document Identifier (including Rev. No. and Change No., if applicable):

ANL-EBS-MD-000004 REV 00

4. Revision/Change No.

5. Description of Revision/Change

00

Initial Issue

CONTENTS

| | Page |
|--|-----------|
| ABBREVIATIONS AND ACRONYMS | 7 |
| 1. PURPOSE | 9 |
| 1.1 ANALYSES AND MODELS REPORT | 9 |
| 1.2 BACKGROUND ON TITANIUM GRADE 7 | 9 |
| 1.3 ENVIRONMENT | 9 |
| 1.4 RELATIONSHIP TO PRINCIPAL FACTORS | 10 |
| 1.5 ACTIVITY PLANS | 10 |
| 1.6 OVERVIEW OF MODEL | 10 |
| 1.7 UNCERTAINTY AND VARIABILITY | 13 |
| 1.8 RESOLUTION OF COMMENTS IN ISSUE RESOLUTION STATUS REPORT ... | 13 |
| 2. QUALITY ASSURANCE (QA) | 16 |
| 3. COMPUTER SOFTWARE AND MODEL USAGE | 16 |
| 3.1 SOFTWARE APPROVED FOR QA WORK | 16 |
| 3.2 INTEGRITY OF TRANSFER OF DATA | 16 |
| 4. INPUTS | 17 |
| 4.1 DATA AND PARAMETERS | 17 |
| 4.1.1 Definition of Parameters | 17 |
| 4.1.2 Determination of Input Parameters | 18 |
| 4.2 CRITERIA | 20 |
| 4.3 CODES AND STANDARDS | 20 |
| 4.3.1 Standard Test Media | 20 |
| 4.3.2 Cyclic Polarization Measurements | 20 |
| 4.3.3 General Corrosion (GC) Measurements | 21 |
| 5. ASSUMPTIONS | 21 |
| 5.1 DRY OXIDATION (DOX) | 21 |
| 5.2 HUMID AIR CORROSION (HAC) | 22 |
| 5.3 AQUEOUS PHASE CORROSION (APC) | 22 |
| 5.4 DRIPPING CONDENSATE FROM INNER SURFACE OF DRIP SHIELD | 22 |
| 5.5 FLOW THROUGH OPENINGS BETWEEN DRIP SHIELDS | 23 |
| 5.6 THRESHOLD FOR LOCALIZED CORROSION (LC) | 23 |
| 5.7 EFFECT OF GAMMA RADIOLYSIS ON CORROSION POTENTIAL | 24 |
| 5.8 MICROBIAL GROWTH | 24 |
| 5.9 PHASE INSTABILITY | 24 |
| 6. ANALYSIS/MODEL | 25 |
| 6.1 DRY OXIDATION | 25 |
| 6.2 HUMID AIR CORROSION | 30 |
| 6.3 AQUEOUS PHASE CORROSION | 31 |

CONTENTS (Continued)

| | Page |
|---|-------------|
| 6.4 LOCALIZED CORROSION | 31 |
| 6.4.1 Threshold Potential for Ti Grade 7..... | 31 |
| 6.4.2 Cyclic Polarization in Synthetic Concentrated J-13 Well Waters..... | 31 |
| 6.4.3 Potential Versus Temperature Correlation for Various Test Media..... | 32 |
| 6.4.4 Correction of Measured Potential for Junction Potential | 41 |
| 6.4.5 Prediction of Critical Temperatures for Pitting and Crevice Corrosion..... | 42 |
| 6.5 RATES OF GENERAL AQUEOUS-PHASE CORROSION | 42 |
| 6.5.1 Corrosion Rates Based Upon Electrochemical Measurements | 42 |
| 6.5.2 Corrosion Rates Based Upon Weight Loss Measurements..... | 49 |
| 6.5.3 Error Analysis for Weight Loss Measurements | 53 |
| 6.5.4 Composite Representation of General Corrosion (GC) Rates for Drip Shield .. | 59 |
| 6.6 DISSOLVED OXYGEN IN THE LONG TERM CORROSION TEST FACILITY .. | 61 |
| 6.7 CREVICE CORROSION..... | 61 |
| 6.8 GAMMA RADIOLYSIS | 62 |
| 6.9 MICROBIALLY INFLUENCED CORROSION | 63 |
| 6.10 MODEL VALIDATION..... | 63 |
| 6.11 SUMMARY OF MODEL | 64 |
| | |
| 7. CONCLUSIONS | 64 |
| | |
| 8. INPUTS AND REFERENCES | 66 |
| 8.1 DOCUMENTS CITED | 66 |
| 8.2 CODES, STANDARDS, REGULATIONS, AND PROCEDURES | 69 |
| 8.3 SOURCE DATA | 70 |

FIGURES

| | Page |
|---|-------------|
| Figure 1. Schematic Representation of Corrosion Model for Titanium Grade 7 Drip Shield ... | 12 |
| Figure 2. Deliquescence Point for Sodium Nitrate Solutions | 19 |
| Figure 3. Regression Analysis of Dry Oxidation Rate Data for Titanium | 29 |
| Figure 4. Determination of Rate Constant as Function of Temperature | 29 |
| Figure 5. Determination of Maximum Oxide Thickness as Function of Temperature | 30 |
| Figure 6. Titanium Grade 7 in SSW at 120°C (NEA031s) | 34 |
| Figure 7. Titanium Grade 7 in SAW at 90°C (NEA025) | 34 |
| Figure 8. Titanium Grade 7 in SCW at 90°C (NEA029) | 35 |
| Figure 9. Titanium Grade 7 in SCW at 60°C (NEA019) | 35 |
| Figure 10. Titanium Grade 7 in SCW at 90°C (NEA003) | 36 |
| Figure 11. Corrosion and Threshold Potentials of Titanium Grade 7 in SSW (NEA031s) | 39 |
| Figure 12. Corrosion and Threshold Potentials for Titanium Grade 7 in SAW | 39 |
| Figure 13. Corrosion and Threshold Potentials for Titanium Grade 7 in SCW | 40 |
| Figure 14. Corrosion and Threshold Potentials for Titanium Grade 7 in SDW | 40 |
| Figure 15. Corrosion and Passive Currents for Titanium Grade 7 in SSW | 46 |
| Figure 16. Corrosion and Passive Currents for Titanium Grade 7 in SAW | 46 |
| Figure 17. Corrosion and Passive Currents for Titanium Grade 7 in SCW | 47 |
| Figure 18. Corrosion and Passive Currents for Titanium Grade 7 in SDW | 47 |
| Figure 19. Distribution of General Corrosion Rates of Ti Grade 16: LTCTF 12-Month Wt. Loss Samples | 52 |
| Figure 20. Distribution of General Corrosion Rates of Ti Grade 16: LTCTF 12-Month Crevice Samples | 52 |
| Figure 21. Distribution of General Corrosion Rates of Ti Grade 16: LTCTF 12-Month Weight Loss and Crevice Samples—No Negative Rates | 59 |
| Figure 22. Distribution of Logarithm of General Corrosion Rates of Ti Grade 16: LTCTF 12-Month Weight Loss and Crevice Samples—No Negative Rates | 60 |

TABLES

| | Page |
|---|-------------|
| Table 1. Data Taken from Reference..... | 28 |
| Table 2. Parameters in Dry Oxidation Rate Equation Determined by Regression Analysis..... | 28 |
| Table 3. Composition of Standard Test Media Based upon J-13 Well Water | 32 |
| Table 4a. Summary of Cyclic Polarization Data for Titanium Grade 7 in Repository-Relevant Conditions (SDW) | 37 |
| Table 4b. Summary of Cyclic Polarization Data for Titanium Grade 7 in Repository-Relevant Conditions (SAW) | 38 |
| Table 5. Summary of Correlated Corrosion and Threshold Potential Data..... | 41 |
| Table 6. Values of E_{corr} and $E_{critical}$ Derived From Correlated Cyclic Polarization Data..... | 41 |
| Table 7. Summary of Junction Potential Corrections for Cyclic Polarization (Volts)..... | 42 |
| Table 8. Conversion of Current Density to Corrosion (Penetration) Rate | 45 |
| Table 9. Conversion of Current Density to Corrosion Rate as Function of Alloy Composition | 45 |
| Table 10. Coefficients for Regression Equations Used to Represent Corrosion and Passive Currents..... | 48 |
| Table 11. Summary of Error Analysis for Corrosion Rates Based Upon Weight Loss Measurements | 54 |
| Table 12. Error Analysis for LTCTF Corrosion Rates–Definitions..... | 55 |
| Table 13. Error Analysis for LTCTF Corrosion Rates–Assume Weight Loss of 0.0001 Grams. | 56 |
| Table 14. Error Analysis for LTCTF Corrosion Rates–Assume Weight Loss of 0.001 Grams... | 57 |
| Table 15. Error Analysis for LTCTF Corrosion Rates–Assume Weight Loss of 0.01 Grams..... | 58 |
| Table 16. Assumed Distribution of Localized Corrosion Rates for Ti Grade 7..... | 62 |

ABBREVIATIONS AND ACRONYMS

| | |
|--------|--|
| AFM | atomic force microscope or microscopy |
| AMR | analyses and models report |
| AP | activity plan |
| APC | aqueous phase corrosion |
| ASTM | American Society for Testing and Materials |
| BSW | basic saturated water |
| CDF | cumulative distribution function |
| CLST | container life and source term |
| CP | cyclic polarization |
| CRM | corrosion resistant material |
| CRWMS | Civilian Radioactive Waste Management System |
| DIS | data inventory sheet |
| DOX | dry oxidation |
| DS | drip shield |
| DTN | data tracking number |
| EBS | engineered barrier system |
| EDA | engineering design alternative |
| EDA II | engineering design alternative number two-second option considered |
| GC | general corrosion |
| HAC | humid air corrosion |
| HIC | hydrogen induced cracking |
| HLW | high-level waste |
| IRSR | issue resolution status report |
| KTI | key technical issue |
| LADS | license application design selection |
| LC | localized corrosion |
| LLNL | Lawrence Livermore National Laboratory |
| LTCTF | Long Term Corrosion Test Facility |
| MIC | microbial influenced corrosion |
| M&O | Management and Operating Contractor |
| NFE | near field environment |
| NHE | normal hydrogen electrode |

ABBREVIATIONS AND ACRONYMS (Continued)

| | |
|--------|---|
| OCRWM | Office of Civilian Radioactive Waste Management |
| PMR | process model report |
| PREN | pit resistance equivalence number |
| PTFE | polytetrafluoroethylene (Teflon) |
| Q | quality data or data qualified for use |
| QA | quality assurance |
| QARD | quality assurance requirements document |
| QP | quality procedure |
| RH | relative humidity |
| SAW | simulated acidic concentrated water |
| SCC | stress corrosion cracking |
| SCE | saturated calomel electrode |
| SCMW | simulated cement-modified water |
| SCW | simulated concentrated water |
| SDW | simulated dilute water |
| SEM | scanning electron microscopy |
| SIMS | secondary ion mass spectrometry |
| SIP | scientific investigation plan |
| SNF | spent nuclear fuel |
| SN | scientific notebook |
| SSW | simulated saturated water |
| TBV | to be verified |
| TDMS | technical data management system |
| TDP | technical development plan |
| TEM | transmission electron microscopy |
| TSPA | Total System Performance Assessment |
| UNS | Unified Numbering System |
| WAPDEG | waste package degradation code |
| WF | waste form |
| WP | waste package |
| WPD | Waste Package Department |
| WPOB | waste package outer barrier |
| wt. % | weight percent |
| XPS | X-ray photoelectron spectroscopy |
| XRD | X-ray diffraction |
| YMP | Yucca Mountain Project |

1. PURPOSE

1.1 ANALYSES AND MODELS REPORT

As described in the license application design selection (LADS) report, the recommended waste package (WP) design is engineering design alternative number two (EDA II) (CRWMS M&O 1999a). This design includes a double-wall WP underneath a protective drip shield (DS).

The purpose of the process-level model described here is to account for both general corrosion (GC) and localized corrosion (LC) of the DS, which is a titanium alloy. Other alloys have been considered in the past, and may again be considered in the future. In regard to GC and LC, Ti Grade 16 is an appropriate analog for Ti Grade 7. No Ti Grade 7 was available for testing. The DS provides protection for the WP outer barrier (WPOB). This model will include several sub-models, which will account for dry oxidation (DOX), humid air corrosion (HAC), GC in the aqueous phase, and LC in the aqueous phase. This analyses and models report (AMR) serves as a feed to the WP process model report (PMR) and the WP degradation (WAPDEG) analyses, and was developed in accordance with the Development Plan work direction (CRWMS M&O 1999b).

The analyses contained in this AMR serve as a basis to determine whether or not the performance requirements for the DS can be met.

1.2 BACKGROUND ON TITANIUM GRADE 7

Alloy 22 is used as the corrosion resistant WPOB. Stainless steel 316NG is to be used for construction of the structural support underneath the WPOB. The 316NG inner cylinder will increase the overall strength of the WP. Titanium alloys are now being considered for construction of the DS. The current recommendation is to use Ti Grade 7 [UNS R52400; 0.03% N (max.), 0.10% C (max.), 0.015% H (max.), 0.25% O (max.), 0.30% Fe (max.), 0.12-0.25% Pd (max.), 0.1% Residuals (max.), 0.4% Residuals (total), and Ti (balance)]. Properties and performance of these materials are reviewed elsewhere (CRWMS M&O 1999e, 2000a). The unusual corrosion resistance of titanium alloys is apparently due to the formation of a passive film of TiO_2 , which is stable over a relatively wide range of potential and pH (Pourbaix 1974). A similar material, Ti Grade 16 with 0.04 to 0.08 % Pd, is used as an analog for Ti Grade 7 in some parts of the testing program. Corrosion tests of Ti Grade 16 have been conducted in the Yucca Mountain Project's (YMP's) Long Term Corrosion Test Facility (LTCTF) (Estill 1998). Test media used in this facility include simulated acidic concentrated water (SAW), which is about one-thousand times more concentrated than the ground water at some distance from Yucca Mountain (J-13 well water) (Harrar et al. 1990), and has been acidified to a pH of approximately 2.7. The rates of GC and oxidation of this material have been shown to be very low. Cyclic polarization (CP) studies have been done with Ti Grade 7.

1.3 ENVIRONMENT

The DS will experience a wide range of conditions during its service life. Initially, the underlying high-level waste (HLW) containers will be relatively hot. The DS surface may be kept dry initially due to the heat generated from radioactive decay. The temperature will drop

eventually to levels where both HAC and aqueous phase corrosion (APC) will be possible. Crevices will be formed between the DS and its invert support structure. Crevices may also form between the DS and mineral precipitates, corrosion products, dust, rocks, cement and biofilms. If the DS settles or collapses, crevices may even form with the WP. The crevice environment may be more severe than the near field environment (NFE). The hydrolysis of dissolved metal can lead to the accumulation of H^+ and a corresponding decrease in pH. Field-driven electromigration of various anions into the crevice must occur to balance cationic charge associated with H^+ ions (Gartland 1997; Walton et al. 1996; Shoesmith et al. 1995). These exacerbated conditions can set the stage for subsequent attack of this corrosion resistant material (CRM) by passive corrosion, pitting, hydrogen induced cracking (HIC), stress corrosion cracking (SCC), or other mechanisms. *Passive corrosion* implies very slow dissolution through a stable passive film. The passive corrosion rate is that which corresponds to the passive current density. Both SCC and LC may also occur outside the crevice.

1.4 RELATIONSHIP TO PRINCIPAL FACTORS

Degradation of the DS is key to understanding one of the most important contributing factors in repository performance. This principal factor is the flow of water through openings in the DS caused by corrosion or ground movement to the outer surface of the WP. This flux of water will ultimately determine the rate of release of radionuclides out. The release rate of radionuclides from the WP will be proportional to the radionuclide concentration multiplied by the flow of water through the WP. Once water contacts (touches) the surface of the WP, its fate becomes intertwined with that of the WP. The models and supporting experimental data to account for both DS and WP degradation, as well as the fate of water involved in the various degradation processes, have been developed by Waste Package Department (WPD). The AMRs comprising the WP PMR address the development of realistic models to account for the degradation of the outer barrier of both the DS and WP, based upon data generated by the YMP. Such tests have been conducted in the YMP's LTCTF (Estill 1998).

1.5 ACTIVITY PLANS

Approved activity plans and technical development plans were used in the performance of the work described in this document. Any necessary deviations from these activity plans are documented in the corresponding scientific notebooks (SNs). These procedures are compliant to the Office of Civilian Radioactive Waste Management (OCRWM) quality assurance (QA) requirements.

1.6 OVERVIEW OF MODEL

The model for the GC and LC of the Ti Grade 7 DS is summarized in [Figure 1](#). The threshold RH is first used to determine whether or not DOX will take place. If DOX is determined to occur, the logarithmic growth law is used to calculate the corrosion rate as a function of temperature. This is discussed in greater detail in Section 6.1. If the threshold RH is exceeded, HAC will occur in the absence of dripping water, and APC will occur in the presence of dripping water. Acceptability is defined as a condition where no LC occurs. If APC is assumed to occur, the corrosion and critical potentials are used to determine whether the mode of attack is general or localized. If the comparison of E_{corr} to $E_{critical}$ indicates GC, the distribution of rates

determined from the LTCTF will be used as the basis of the GC rate. This model does not account for the effects of microbial growth or aging on corrosion rates.

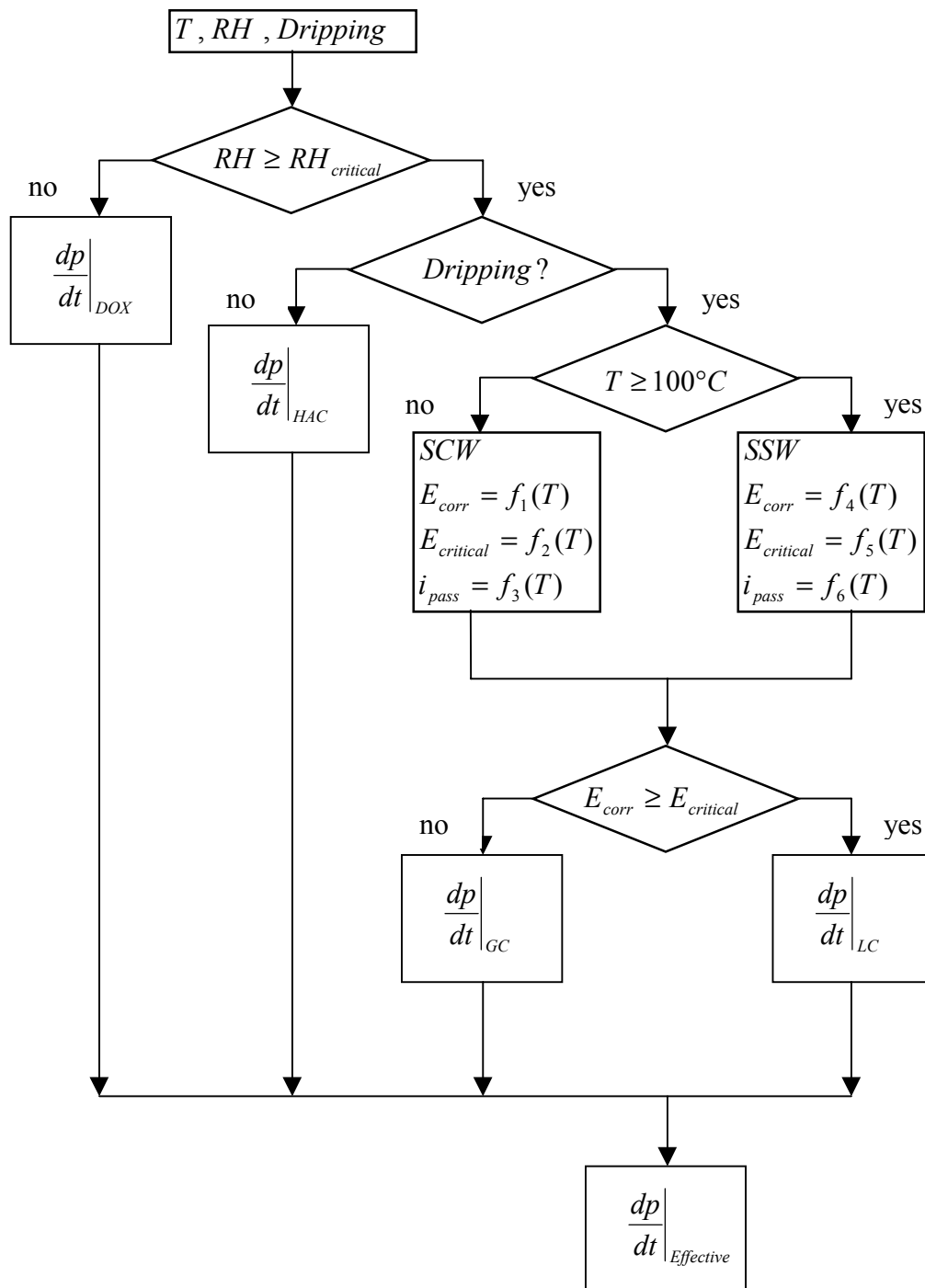


Figure 1. Schematic Representation of Corrosion Model for Titanium Grade 7 Drip Shield

1.7 UNCERTAINTY AND VARIABILITY

The primary uncertainty in the threshold RH for HAC and APC is due to the presence of nitrate. Values of the equilibrium RH as a function of temperature for a saturated solution of NaNO_3 are given in Table 9 and Figure 8 of the AMR on DS and WP surface environments (CRWMS M&O 2000a). Despite significant experimental work at Lawrence Livermore National Laboratory (LLNL), there continues to be significant uncertainty in the threshold RH for HAC and APC.

In an ideal case, the crevice corrosion temperature can be estimated from the intersection of the lines representing the corrosion and threshold potentials at elevated temperature. To force crevice corrosion to occur in the model, E_{corr} and $E_{critical}$ can simply be equated over temperature ranges of uncertainty (90-120°C). It is assumed that the crevice corrosion temperature is uniformly distributed over this range of uncertainty. Additional data is needed to fill this void.

From the data given in Section 6.5, the uncertainty in GC rates for Ti Grade 16, which is an appropriate analog for Ti Grade 7, can be estimated. In the case of samples with generic weight loss geometry, measured GC rates are shown in Figure 19. The distribution of measured rates appears to be symmetric and centered close to zero. The maximum and minimum rates fall within the limit defined by $\pm 200 \text{ nm y}^{-1}$. In the case of samples with generic crevice geometry, measured GC rates are shown in Figure 20. The distribution of measured rates appears to be slightly asymmetric, but still centered close to zero. The maximum and minimum rates fall within the limit defined by $\pm 350 \text{ nm y}^{-1}$. The negative rates could be due to either scale formation or oxidation of the titanium.

It is assumed that no scale formation occurs, so all negative rates are eliminated and the entire distribution is assumed to be due to uncertainty. As shown in Section 6.5.2, the rate at the 50th percentile is approximately 25 nm y^{-1} , the rate at the 90th percentile is approximately 100 nm y^{-1} , and the maximum rate is 350 nm y^{-1} . About 10% of the values fall between 100 and 350 nm y^{-1} .

1.8 RESOLUTION OF COMMENTS IN ISSUE RESOLUTION STATUS REPORT

The issue resolution status report (IRSR) recently issued by the NRC (1999) provides guidance for the development of process-level models. The primary consideration in the key technical issue (KTI) is the container life and source term (CLST). There must be a high degree of confidence in the adequacy of the engineered barrier system (EBS) design, thereby providing assurance that containers will be adequately long-lived, and radionuclide releases from the EBS will be sufficiently controlled. The container design and the packaging of spent nuclear fuel (SNF) and HLW glass are expected to make a significant contribution to the overall repository performance. The IRSR defines the physical boundary of the EBS by the walls of the WP emplacement drifts. The IRSR deems six sub-issues to be important to the resolution of the KTI. The first sub-issue is specifically relevant to this AMR: the effects of corrosion processes on the lifetime of the containers.

The acceptance criteria for sub-issue 1 are:

1. DOE has identified and considered likely modes of corrosion for container materials, including dry-air oxidation, humid-air corrosion, and aqueous corrosion processes, such as GC, LC, MIC, SCC, and HIC, as well as the effect of galvanic coupling.

Response: This AMR includes process-level models for DOX, HAC, and APC processes, such as GC, LC and MIC. Galvanic coupling effects have been minimized to the extent possible, and will be accounted for in greater detail in future revisions. Both stress corrosion cracking and hydrogen embrittlement are dealt with in companion AMRs.

2. DOE has identified the broad range of environmental conditions within the WP emplacement drifts that may promote the corrosion processes listed previously, taking into account the possibility of irregular wet and dry cycles that may enhance the rate of container degradation.

Response: This AMR includes environmental thresholds that can be used to switch between dominant modes of corrosion. For example, as the WP temperature drops and the RH increases, the mode of attack changes from dry-air oxidation to humid-air or aqueous-phase corrosion. A comparison of the corrosion and threshold potentials is used to determine whether or not LC will occur.

3. DOE has demonstrated that the numerical corrosion models used are adequate representations, taking into consideration associated uncertainties, of the expected long-term behaviors and are not likely to underestimate the actual degradation of the containers as a result of corrosion in the repository environment.

Response: Uncertainties are accounted for in corrosion rates. From the data given in Section 6.5, the uncertainty in GC rates for Ti Grade 16, which is assumed to be an appropriate analog for Ti Grade 7, can be estimated. In the case of samples with generic weight loss geometry, measured GC rates are shown in Figure 19. The distribution of measured rates appears to be symmetric and centered close to zero. The maximum and minimum rates fall within the limit defined by $\pm 200 \text{ nm y}^{-1}$. In the case of samples with generic crevice geometry, measured GC rates are shown in Figure 20. The distribution of measured rates appears to be slightly asymmetric, but still centered close to zero. The maximum and minimum rates fall within the limit defined by $\pm 350 \text{ nm y}^{-1}$. The negative rates could be due to either scale formation or oxidation of the titanium. It is assumed that no scale formation occurs, so all negative rates are eliminated and the entire distribution is assumed to be due to uncertainty. As shown in Section 6.5.2, the rate at the 50th percentile is approximately 25 nm y^{-1} , the rate at the 90th percentile is approximately 100 nm y^{-1} , and the maximum rate is 350 nm y^{-1} . About 10% of the values fall between 100 and 350 nm y^{-1} .

4. DOE has considered the compatibility of container materials, the range of material conditions, and the variability in container fabrication processes, including welding, in assessing the performance expected in the containers intended waste isolation.

Response: It is believed that Ti Grade 7 is a stabilized alpha (α) phase alloy. At the temperatures expected in the repository, this single-phase material is assumed to have outstanding phase stability. Poor atmospheric conditions during welding could lead to internal oxidation of the material. Environmental conditions that could dissolve TiO_2 could lead to localized attack associated with the internal oxidation. It is believed that this material is essentially immune to MIC. This model does not yet account for the effects of microbial growth or aging on corrosion rates. However, such enhancements of the corrosion rate will be accounted for in the future.

5. DOE has justified the use of data collected in corrosion tests not specifically designed or performed for the Yucca Mountain repository program for the environmental conditions expected to prevail at the YM site.

Response: The threshold RH used to determine whether vapor phase attack is by DOX or HAC is based upon the deliquescence point of salt deposits that could form on the WP surface due to aerosol transport. Measurements of GC rates in the vapor and aqueous phases, electrochemical potentials, and other relevant performance data were in test media that can be directly related to water chemistry expected on the DS surface during the service life of Ti Grade 7. These water chemistries are based upon evaporative concentrations of the standard J-13 well water chemistry. Crevice chemistry is being measured in situ, with and without the presence of buffer ions. In the aqueous phase, a range of temperature extending from room temperature to 120°C is being investigated. The high-temperature limit is based upon the boiling point of a near-saturation water chemistry without buffer. The expected boiling point of the aqueous phase on the WP surface is expected to be lower.

6. DOE has conducted a consistent, sufficient, and suitable corrosion testing program at the time of the LA submittal. In addition, DOE has identified specific plans for further testing to reduce any significant area(s) of uncertainty as part of the performance confirmation program.

Response: The DOE has established a corrosion test program that addresses all anticipated modes of corrosive attack of the WP. Studies include exposure of over 18,000 samples of candidate WP material in the LTCTF. A large number of pre- and post-exposure measurements of dimension and weight allow establishment of distribution functions for representation of the GC rate. Microscopic examination of samples from the LTCTF and other corrosion tests is done with scanning electron microscopy (SEM), atomic force microscopy (AFM), X-ray diffraction (XRD), X-ray photoelectron spectroscopy (XPS), secondary ion mass spectrometry (SIMS), and other state-of-the-art surface analytical techniques. Potentiodynamic and potentiostatic electrochemical tests are conducted with base metal, thermally aged material, and simulated welds. Thermally aged material is fully characterized with the transmission electron microscope (TEM) (CRWMS M&O 2000b).

7. DOE has established a defensible program of corrosion monitoring and testing of the engineered subsystems components during the performance confirmation period to assure they are functioning as intended and anticipated.

Response: The DOE has established a corrosion test program that addresses all anticipated modes of corrosive attack of the WP. There is a clear linkage between the experimental data being collected and modules in the predictive WAPDEG code that serves as the heart of the Total System Performance Assessment (TSPA). Data and modules have been developed for each key element of the EDA II design: the WPOB (Alloy 22); the inner structural support (stainless steel 316NG); and the protective DS (Ti Grade 7). Companion AMRs provide data and modules for the stainless steel 316NG and the Ti Grade 7 alloy.

2. QUALITY ASSURANCE (QA)

The QA program applies to this analysis. The drip shield was classified (per QAP-2-3) as Quality Level-1 in *Classification of the MGR Ex-Container System* (CRWMS M&O 1999c, p. 8). The development of this analysis is conducted under activity evaluation *11017040 Long Term Materials Testing and Modeling* (CRWMS M&O 1999d) which was prepared per QAP-2-0. The results of that evaluation were that the activity is subject to the *Quality Assurance Requirements and Description* (DOE 2000) requirements.

3. COMPUTER SOFTWARE AND MODEL USAGE

3.1 SOFTWARE APPROVED FOR QA WORK

Calculations used to manipulate raw data were performed electronically in spreadsheets created with Microsoft Excel 97 using built-in functions. The Microsoft Excel 97 that was used was bundled with Microsoft Office 97 Professional Edition for Windows 95/NT or Workstation 4.0 (SN # 269-056-174). Excel is considered commercially available software from the OCRWM procedure entitled *Software Management* (AP-SI.1Q).

3.2 INTEGRITY OF TRANSFER OF DATA

The integrity of electronic data transfer has been verified as required by OCRWM Procedure YAP-SV.1Q. The comparison method was used to ensure the accuracy of the transferred data. A sampling of approximately 5% of the data in the source file was visually compared to the corresponding data in the transferred file. The data selected was at the reviewer's discretion. Reviewers included the originator, as well as the document editor and QA staff.

4. INPUTS

4.1 DATA AND PARAMETERS

4.1.1 Definition of Parameters

| | |
|-----------------|--|
| a | dimension of weight loss sample |
| b | dimension of weight loss sample |
| c | dimension of weight loss sample |
| Δa | change in a |
| Δb | change in b |
| Δc | change in c |
| b_0 | coefficient in regression equation |
| b_1 | coefficient in regression equation |
| b_2 | coefficient in regression equation |
| $f(y)$ | probability density function |
| i_{corr} | corrosion current density |
| i_{pass} | passive current density |
| k | rate constant in DOX model |
| k_0 | pre-exponential constant in DOX model |
| p | wall penetration due to corrosive attack |
| t | exposure time during weight loss measurement |
| t | time in DOX model |
| u_i | mobility of the i^{th} ion |
| w | measured weight loss |
| Δw | change in w |
| w_{oxide} | formula weight of oxide formed during DOX |
| x | independent variable in regression equation |
| x_i | measured parameter in sensitivity (error) analysis |
| y | dependent variable in regression equation |
| y | computed value in sensitivity (error) analysis |
| z_i | valence (charge) of the i^{th} ion |
| $C_i(\alpha)$ | molar concentration of the i^{th} ion in alpha phase |
| $C_i(\beta)$ | molar concentration of the i^{th} ion in the beta phase |
| D_{oxide} | diffusivity of reacting species through protective oxide |
| E_a | Arrhenius activation energy |
| E_{corr} | corrosion potential |
| $E_{critical}$ | critical potential – threshold for localized attack |
| E_j | junction potential – correction for reference electrode junction |
| F | Faraday's constant |
| J_{oxide} | flux of reacting species through protective oxide |
| R | universal gas constant |
| R^2 | regression coefficient |
| RH | relative humidity |
| $RH_{critical}$ | threshold RH for HAC |

| | |
|-----------------|--|
| T | temperature (degrees Celsius or Kelvin, depending upon equation) |
| X | oxide thickness in DOX model |
| X_{max} | apparent maximum oxide thickness in DOX model |
| σ | standard deviation |
| μ | mean |
| ρ | density of Ti Grade 7 |
| $\Delta\rho$ | change in ρ |
| ρ_{oxide} | density of oxide formed during DOX |
| ζ_{oxide} | stoichiometric coefficient for DOX reaction |

4.1.2 Determination of Input Parameters

Input for this AMR includes bounding conditions for the local environment on the WP surface, which include temperature, relative humidity (RH), presence of liquid-phase water, liquid-phase electrolyte concentration (chloride, buffer, and pH), and oxidant level. The detailed evolution of the environment on the WP surface is defined by a companion AMR entitled *Environment on the Surface of Drip Shield and Waste Package Outer Barrier* (CRWMS M&O 2000a). This work has been used to define the threshold RH for HAC and APC, as well as a medium for testing DS and WP materials under what is now believed to be a worst-case scenario. This test medium is presented here as simulated saturated water (SSW) and has a boiling point of approximately 120°C.

In the AMR on WP environment (CRWMS M&O 2000a), hygroscopic salts may be deposited by aerosols and dust introduced with the backfill. They will be dissolved in seepage water that enters the drifts and the episodic water that flows through the drifts. Salts will be deposited on the WP surface during evaporation. Such hygroscopic salts, deposited on WP surfaces, enable aqueous solutions to exist as thin surface films at relative humidities below 100%. The threshold RH ($RH_{critical}$) at which a thin-film aqueous solution can exist on the surface is defined as the deliquescence point (CRWMS M&O 2000a). The threshold RH ($RH_{critical}$) at which an aqueous solution can exist is defined as the deliquescence point (CRWMS M&O 2000a). This threshold defines the condition necessary for aqueous electrochemical corrosion processes of a metal with salt deposits to occur at a given temperature. Other ions may be present but at significantly lower levels. The deliquescence point of NaCl is relatively constant with temperature and varies from 72-75%. In contrast, the deliquescence point of NaNO₃ has a strong dependence on temperature, ranging from an RH of 75.36% at 20°C to 65% at 90°C. The temperature dependence of RH is represented by Equation 1. The implied equilibrium RH is 50.1% at 120.6°C. The primary uncertainty in the threshold RH for HAC and APC is due to the presence of nitrate. Values of the equilibrium RH as a function of temperature for a saturated solution of NaNO₃ are given in the AMR on DS and WP surface environments. It has been shown that any other salts with lower deliquescence points ($RH_{critical}$) are precipitated (CRWMS M&O 2000a). This threshold obeys the following polynomial in temperature, which is a fit of the data deliquescence point data for NaNO₃:

$$RH_{critical} = -3.5932 \times 10^{-5} \times T(^{\circ}C)^3 + 5.9649 \times 10^{-3} \times T(^{\circ}C)^2 - 0.45377 \times T(^{\circ}C) + 81.701 \quad (\text{Eq. 1})$$

$$R^2 = 0.9854,$$

where R^2 is the coefficient of determination and where R is the coefficient of correlation. This correlation is compared to the data in Figure 2.

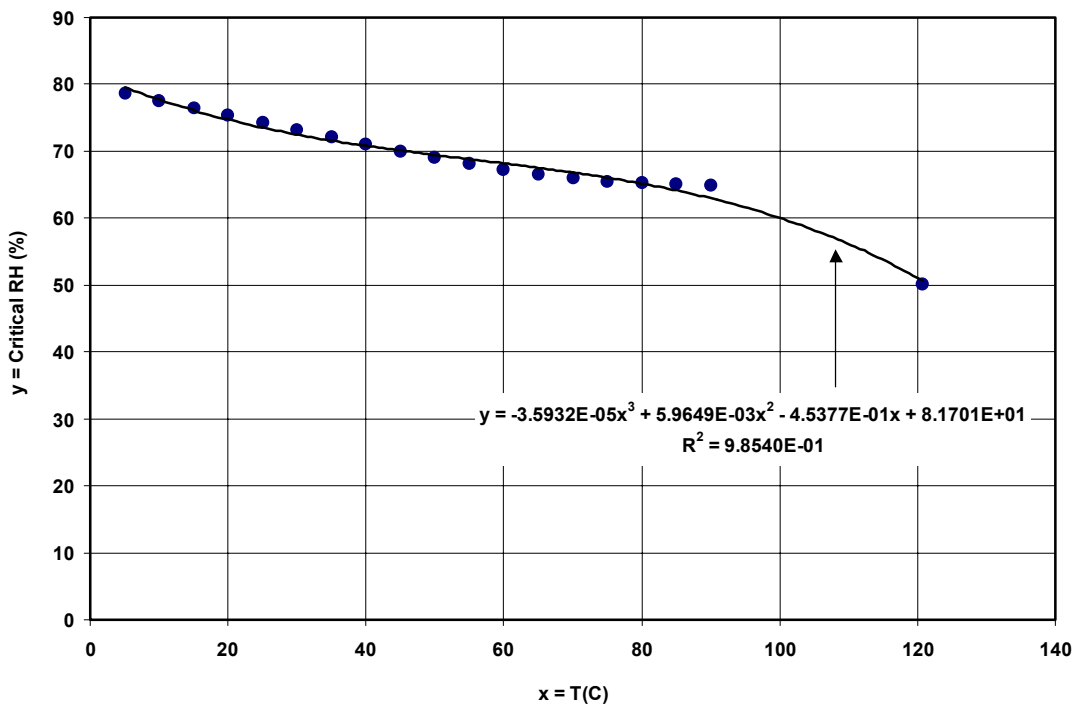


Figure 2. Deliquescence Point for Sodium Nitrate Solutions

As pointed out by CRWMS M&O (2000a), the deliquescence point can cover a broad range. For example, the deliquescence point of NaOH is 1.63% at 75°C. The deliquescence point of K₂SO₄ is 97.59% at 20°C. It is assumed that the uncertainty in $RH_{critical}$ can be represented by a triangular distribution (Section 6.5.4). The value at the 50th percentile is represented by Equation 1. Values at the 0th and 100th percentiles are assumed to be 1.63 and 97.59%, respectively. The specified bounds represent possible binary combinations of anions and cations in J-13 well water. This range addresses concerns regarding a possible lack of conservatism raised during auditing of other related AMRs.

As discussed in the AMR on WP environment (CRWMS M&O 2000a), the evaporation of J-13 well water near the boiling point results in the concentration of Na⁺, K⁺, Cl⁻, and NO₃⁻. The concentration of HCO₃⁻ reaches a constant level while the concentrations of F⁻ and SO₄²⁻ initially increase, but eventually fall, due to precipitation. Ultimately, the F⁻ drops below the level of detection. The SSW used for testing is an abstract embodiment of this observation. The SSW formulation is based upon the assumption that evaporation of J-13 well water eventually leads to a sodium-potassium-chloride-nitrate solution. The absence of sulfate and carbonate in this test medium is believed to be conservative, in that carbonate would help buffer pH in any occluded geometry such as a crevice. Polyprotic anions with multistep dissociation tend to serve as buffers.

Experimental data from the scientific and technical literature, the LTCTF and CP measurements, and crevice corrosion experiments at LLNL are used as a basis for this process-level model. The rationale for the test media in the LTCTF is discussed in Section 6.4.2 below and by Gdowski (UCRL-ID-132287; UCRL-ID-132286; UCRL-ID-132285). Determination of many of the listed parameters is not found specifically in this section but is discussed in detail in Section 6.0, "Analysis/Model." Specific input parameters from the LTCTF are GC rates from the various test media. CP measurements provide corrosion and threshold potentials necessary for switching from one corrosion mode to another (GC to LC). The crevice corrosion experiments enable the crevice pH to be reasonably bounded.

4.2 CRITERIA

The DS is intended to protect the WP, thereby prolonging WP life. Therefore, the DS must help meet criteria specific to the WP.

In addition to the criteria specifically relevant to the WP, criteria for the drip shield have now been developed. *Emplacement Drift System Description Document* (CRWMS M&O 2000d), Design Criterion 1.2.1.12, (p. 10) appears to be the best candidate in supporting this analysis.

The criterion 1.2.1.12 states:

"The drip shield shall have an operating life of 10,000 years."

This criterion is needed to ensure that the drip shield is designed with an operating life long enough to achieve the functions allocated to it.

4.3 CODES AND STANDARDS

4.3.1 Standard Test Media

G. E. Gdowski, Formulation and Make-up of Simulated Dilute Water (SDW), Low Ionic Content Aqueous Solution, Yucca Mountain Project, Lawrence Livermore National Laboratory, Livermore, CA, TIP-CM-06, Revision CN TIP-CM-06-0-2, April 4, 1997, Table 1, p. 3. UCRL-ID-132285.

G. E. Gdowski, Formulation and Make-up of Simulated Concentrated Water (SCW), High Ionic Content Aqueous Solution, Yucca Mountain Project, Lawrence Livermore National Laboratory, Livermore, CA, TIP-CM-07, Revision CN TIP-CM-07-0-2, April 4, 1997, Table 1, pp. 3-4. UCRL-ID-132286.

G. E. Gdowski, Formulation and Make-up of Simulated Acidic Concentrated Water (SAW), High Ionic Content Aqueous Solution, Yucca Mountain Project, Lawrence Livermore National Laboratory, Livermore, CA, TIP-CM-08, Revision CN TIP-CM-08-0-2, April 4, 1997, Table 1, p. 3. UCRL-ID-132287.

4.3.2 Cyclic Polarization Measurements

Standard Practice for Conventions Applicable to Electrochemical Measurements in Corrosion

Testing, Designation G 3-89, 1989 Annual Book of American Society for Testing and Materials (ASTM) Standards, Section 3, Vol. 3.02, pp. 36-44.

Standard Test Method for conducting Cyclic Potentiodynamic Polarization Measurements for Localized Corrosion Susceptibility of Iron-, Nickel-, or Cobalt-Based Alloys, Designation G 61-86, 1997 Annual Book of American Society for Testing and Materials (ASTM) Standards, Section 3, Vol. 3.02, pp. 231-235.

Standard Reference Test Method for Making Potentiostatic and Potentiodynamic Anodic Polarization Measurements, Designation G 5-94, 1997 Annual Book of American Society for Testing and Materials (ASTM) Standards, Section 3, Vol. 3.02, pp. 54-57.

Standard Reference Test Method for Making Potentiostatic and Potentiodynamic Anodic Polarization Measurements, Designation G 5-87, 1989 Annual Book of American Society for Testing and Materials (ASTM) Standards, Section 3, Vol. 3.02, pp. 79-85.

ASTM G48-99a. 1999. *Standard Test Methods for Pitting and Crevice Corrosion Resistance of Stainless Steels and Related Alloys by Use of Ferric Chloride Solution*. West Conshohocken, Pennsylvania: American Society for Testing and Materials.

4.3.3 General Corrosion (GC) Measurements

Standard Practice for Preparing, Cleaning, and Evaluating Corrosion Test Specimens, Designation G 1-90, 1997 Annual Book of American Society for Testing and Materials (ASTM) Standards, Section 3, Vol. 3.02, pp. 15-21.

Standard Practice for Preparing, Cleaning, and Evaluating Corrosion Test Specimens, Designation G 1-81, 1987 Annual Book of American Society for Testing and Materials (ASTM) Standards, Section 3, Vol. 3.02, pp. 89-94, Subsection 8–Calculation of Corrosion Rate, Appendix X1 – Densities for a Variety of Metals and Alloys.

5. ASSUMPTIONS

5.1 DRY OXIDATION (DOX)

DOX of the DS occurs at any RH below the threshold ($RH_{critical}$) for HAC:

$$RH < RH_{critical} \quad (\text{Eq. 2})$$

$RH_{critical}$ is given by Equation 1 CRWMS M&O (2000a) as mentioned in Section 4.1.2. As pointed out by CRWMS M&O (2000a), the deliquescence point can cover a broad range. For example, the deliquescence point of NaOH is 1.63% at 75°C. The deliquescence point of K₂SO₄ is 97.59% at 20°C. The uncertainty in $RH_{critical}$ can be represented by a triangular distribution (Section 6.5.4 of the companion AMR on Alloy 22) (CRWMS M&O 2000c). The value at the 50th percentile is represented by Equation 1. Numerical values at the 0th and 100th percentiles are 1.63 and 97.59%, respectively. The specified bounds represent possible binary combinations of

anions and cations in J-13 well water. In the absence of dripping, nitrate salts could be deposited on the DS surface from entrained dust and other aerosols.

DOX forms an adherent, protective oxide film of uniform thickness. In general, the rate of DOX is limited by mass transport through the growing metal oxide film, and the oxide thickness obeys a logarithmic growth law (Shoosmith et al. 1995). Reasonable values of the logarithmic rate constant have been assumed, as discussed in Section 6.1. This is a reasonably bounding assumption. This assumption is used in the analysis presented in Section 6.1.

5.2 HUMID AIR CORROSION (HAC)

HAC occurs at any RH above the threshold, provided that there is no dripping:

$$RH \geq RH_{critical} \quad (\text{Eq. 3})$$

The rates of HAC and APC can be represented by a combination of data from the LTCTF. It will also be assumed that the GC rate is constant and does not decay with time. Less conservative corrosion models assume that the rate decays with time. HAC is assumed to occur uniformly over each WAPDEG patch, which is comparable in size to that of a LTCTF sample with generic weight-loss geometry. These are reasonably bounding assumptions. They are relevant to the analysis presented in Section 6.2.

5.3 AQUEOUS PHASE CORROSION (APC)

At a given surface temperature, the existence of liquid-phase water on the DS depends upon the presence of a salt and mineral deposit. In the presence of such a deposit, a liquid-phase can be established at a higher temperature than otherwise possible. Two conditions must be met for APC: dripping water, and RH above the deliquescence point of the deposit at the temperature of the DS surface.

$$RH \geq RH_{critical} \quad (\text{Eq. 4})$$

This threshold RH for HAC ($RH_{critical}$) is given by Equation 1, which is based on the AMR entitled *Environment on the Surface of Drip Shield and Waste Package Outer Barrier* (CRWMS M&O 2000a). For the time being, the composition of the electrolyte formed on the DS surface is assumed to be that of simulated concentrated water (SCW) below 100°C, and that of SSW above 100°C. It will be assumed that the GC rate is constant and does not decay with time. Less conservative corrosion models assume that the rate decays with time. General APC is assumed to occur uniformly over each WAPDEG patch, which is comparable in size to that of a LTCTF sample with generic weight-loss geometry. These are reasonably bounding assumptions. These assumptions are used in Section 6.3.

5.4 DRIPPING CONDENSATE FROM INNER SURFACE OF DRIP SHIELD

Once the temperature of the DS drops below the dew point, condensation can occur on the inner surface. While clinging to the underside of the DS, it is assumed that this condensate is

essentially pure water. Ultimately, this condensate can then form droplets that fall and impinge the underlying WP surface, provided that the droplets are sufficiently large so that they can fall through the temperature gradient towards the WP without complete evaporation. Once on the WP surface, the droplets can equilibrate with salt-containing dust on the WP surface, thereby forming a concentrated electrolyte. Measurements made with simulated dilute water (SDW) are used as the basis of model predictions. This is a reasonably bounding assumption. This assumption is relevant to analysis presented in Section 6.3.

5.5 FLOW THROUGH OPENINGS BETWEEN DRIP SHIELDS

It is believed that the final analysis will show that GC does not limit the life of the DS over a 10,000-year period, and that no significant LC occurs. However, ground movement may cause displacement of adjacent drip shields along the drift axis, thereby opening pathways that enable dripping water to reach the WP. For a given mass flow of water contacting the outer surface of the DS, the fraction passing through an opening to the WP is expected to be proportional to the following multiplication factor (Θ_{shield}):

$$\Theta_{shield} = \frac{A_{opening}}{A_{shield}} \quad (\text{Eq. 5})$$

where $A_{opening}$ is the projected area of the opening on the floor of the drift, and A_{shield} is the projected area of the DS on the floor of the drift. Equation 5 relates DS failure to WP degradation and radionuclide transport. Such displacement could also introduce enough stress to cause either SCC or HIC, and a more catastrophic failure of the DS. These are conservative assumptions, because the design of the drip shield will preclude separation under expected seismic loads. This assumption is relevant to analysis presented in Section 6.3.

5.6 THRESHOLD FOR LOCALIZED CORROSION (LC)

If the open circuit corrosion potential (E_{corr}) is less than the threshold potential for localized corrosion (LC) ($E_{critical}$), it will be assumed that no LC occurs.

$$E_{corr} < E_{critical} \quad (\text{Eq. 6})$$

Such assumptions are common in the corrosion literature and are also used in the AMR for Alloy 22 (CRWMS M&O 2000c).

For the time being, it is expected that the entire external surface of the DS has formed a crevice with either rocks or backfill. The pH in this crevice region may be lower than that of the NFE, though no significant LC has been observed in artificial titanium crevices exposed in the LTCTF for 12 months. Therefore, SAW water chemistry with a pH of approximately 2.7 is assumed. The potential verses temperature correlation for SAW should be used to determine whether or not the threshold for LC has been exceeded in this crevice region.

If the threshold potential for localized attack is exceeded, a corrosion rate representative of LC must be assumed. If LC occurs, it is assumed that the rate of attack will be uniform over an entire WAPDEG patch. This would be equivalent to assuming that an entire patch encounters

active crevice corrosion. It is assumed that no individual pits form. Unfortunately, due to the outstanding corrosion resistance of Ti Grade 7, relatively little data exists for such LC under plausible conditions. From the reviewed literature (Gdowski 1997, Table 15.1), a crevice corrosion depth of 250 microns was observed in a crevice formed from Ti-0.2%Pd and PTFE after a 582-day exposure in deaerated brine at 90°C (157 microns per year). In a metal-metal crevice, a crevice corrosion depth of 70 microns was observed in a crevice formed from Ti-0.2%Pd after 489 days (52 microns per year). Other more severe values are also given by Gdowski (1997, Appendix A) and are shown in Table 16 in Section 6.7. This table represents the range of corrosion rates observed in acidic environments, such as those anticipated in crevices. It is expected that a rectangular distribution based on this table is applicable for the LC of Ti Grade 7. Since it is not possible to separate the variability and uncertainty, the two are assumed to be equivalent and represented by Table 16 in the present analysis. In addition, it is assumed that the crevice corrosion temperature is uniformly distributed over the temperature range of uncertainty. The crevice corrosion temperature is the critical crevice corrosion temperature below which crevice corrosion is not possible. Therefore, uniform distribution is conservative. This assumption is used in Section 6.4.

5.7 EFFECT OF GAMMA RADIOLYSIS ON CORROSION POTENTIAL

The primary effect of gamma radiolysis is the generation of hydrogen peroxide, an oxidant. It is assumed that the effects of such oxidants can be accounted for through changes induced on the open circuit corrosion potential (E_{corr}). Based upon published data described in Section 6.8, it is believed that the shift in corrosion potential due to gamma radiolysis is much less than 200 mV, a value measured for stainless steels. This conservative approach has been further discussed in Section 6.8.

5.8 MICROBIAL GROWTH

In the present model, it is assumed that the effect of microbial growth on E_{corr} is not significant. In general, titanium is very resistant to MIC. According to Shoesmith et al. (1995), the initiation of crevice corrosion under bio-films has never been observed for titanium. However, since titanium is not bio-toxic such a process is not ruled out. This is a reasonably bounding assumption and further discussed in Section 6.9.

5.9 PHASE INSTABILITY

The effects of phase instability on degradation of Ti Grade 7 and 16 are expected to be insignificant. Pure titanium is an allotropic element, existing in more than one crystallographic form (Gdowski 1997). Above 883°C it has the body-centered cubic (bcc) crystal structure, which is called the beta (β) phase. Below 883°C, it transforms to a hexagonal close-packed (hcp) structure, which is called the alpha (α) phase. Both Ti Grs 7 and 16 are α -phase alloys and have very small additions of Pd. The solubility of Pd in these materials is about 1 weight percent at 400°C. The nominal concentrations of Pd in both Ti Grs 7 and 16 are well below the solubility limit at this temperature (Gdowski 1997, pp. 1-8). Titanium-palladium intermetallic compounds capable of being formed in this system have not been reported to occur in Ti Grade 7 and 16 with normal heat treatments.

DS temperature is governed by the temperature of the underlying WP. The transition from α - to β -phase titanium should not occur at these temperatures. The cladding on the SNF limits the WP temperature to levels below 350°C. As discussed in the companion AMR on GC and LC of the WPOB (CRWMS M&O 2000c), the WP temperature is further limited to levels below 300°C due to long-term aging effects that might be encountered with Alloy 22. At these low levels, no α - β transition will occur and palladium is well below its solubility limit. No detrimental effect of such a low temperature on the long-term phase stability and phase-dependent corrosion rate is expected. These are basic microstructural information about titanium metal and are relevant to LC (sec. 6.4).

6. ANALYSIS/MODEL

6.1 DRY OXIDATION

DOX occurs at any RH below the threshold for HAC.

$$RH < RH_{critical} \quad (\text{Eq. 7})$$

This process results in the formation of an adherent, protective oxide film of uniform thickness. The protective oxide film is primarily TiO_2 . The oxidation reaction is given as (Welsch et al. 1996):



The rate of DOX is limited by mass transport through this growing metal oxide film. Fick's first law is applied, assuming a linear concentration gradient across the oxide film of thickness x :

$$J_{oxide} = -D_{oxide} \frac{\partial C}{\partial x} \approx -D_{oxide} \frac{\Delta C}{x} \quad (\text{Eq. 9})$$

where J_{oxide} is the molar flux of the reacting species in the oxide, D_{oxide} is the diffusivity of the reacting species in the oxide, ΔC is the corresponding differential molar concentration. Oxide growth is related to the flux by:

$$\frac{dx}{dt} = \frac{\zeta_{oxide} \times w_{oxide} \times J_{oxide}}{\rho_{oxide}} \quad (\text{Eq. 10})$$

where ζ_{oxide} is the stoichiometric coefficient (moles of oxide per mole of diffusing species), w_{oxide} is the formula weight of the oxide, and ρ_{oxide} is the density of the oxide. Integration shows that the oxide thickness should obey the following parabolic growth law (Wagner's Law) (Welsch et al. 1996), where the film thickness is proportional to the square root of time:

$$x = \sqrt{x_0^2 + k \times t} \quad (\text{Eq. 11})$$

where x_0 is the initial oxide thickness, x is the oxide thickness at time t , and k is a temperature-dependent parabolic rate constant. More specifically, k is defined as follows:

$$k = \frac{2 \times \zeta_{oxide} \times w_{oxide} \times D_{oxide} \times \Delta C}{\rho_{oxide}} \quad (\text{Eq. 12})$$

In this particular case (Equations 11 and 12), the rate constant k has the units $\text{cm}^2 \text{s}^{-1}$, the same as diffusivity. At high temperature (600-900°C), published values of k_{pw} could be used to calculate k (Welsch et al. 1996).

As pointed out by Shoesmith et al. (1995), oxide thickening on Ti Grade 7 in groundwater-saturated bentonite at 95°C obeys the logarithmic growth law (Shoesmith et al. 1995, pp. 9-11). Such kinetics are also evident for the growth of thermal oxide films on unalloyed titanium in air at 400 to 600°C (Pohlman 1987, p. 685, Fig. 25). The data as read from the original figure is given in [Table 1](#). The logarithmic growth law is represented by Equation 13 below:

$$\ln(1 - X / X_{max}) = -k t \quad (\text{Eq. 13})$$

where X is the oxide thickness in nanometers, t is time in minutes and k is a rate constant with the units of inverse time (min^{-1}). Note that the rate constant in Equations 11 and 12 is different from the one in Equation 13. The estimated maximum oxide thickness is X_{max} . Equation 13 can be rewritten as:

$$X = X_{max} (1 - e^{-k t}) \quad (\text{Eq. 14})$$

The rate is then:

$$\frac{dX}{dt} = k e^{-k t} \quad (\text{Eq. 15})$$

A slight modification of Equation 13 allows one to account for some oxide on the titanium at zero time. More specifically, the intercept on the time axis, t_0 , is the point at which the oxide thickness would have been zero.

$$\ln(1 - X / X_{max}) = -k t + k t_0 \quad (\text{Eq. 16})$$

The parameters in [Table 2](#) were determined by the linear regression analysis shown in [Figure 3](#). The rate constant, k , obeys the Arrhenius equation:

$$k = k_0 e^{-E_a / RT} \quad (\text{Eq. 17})$$

where k_0 is a constant, E_a is the activation energy, R is the universal gas constant, and T is the absolute temperature. The activation energy can be determined by comparing values of k at two temperatures, as shown in Equations 6 or 7:

$$\frac{k_1}{k_2} = \frac{e^{-E_a R/T_1}}{e^{-E_a R/T_2}} \quad (\text{Eq. 18})$$

$$\ln\left(\frac{k_1}{k_2}\right) = -\frac{E_a}{R} \left(\frac{1}{T_1} - \frac{1}{T_2}\right) \quad (\text{Eq. 19})$$

Values from [Table 2](#) for 400 and 500°C can be substituted into Equation 19 to give:

$$\ln\left(\frac{0.0345}{0.0538}\right) = -\frac{E_a}{R} \left(\frac{1}{773\text{ K}} - \frac{1}{673\text{ K}}\right)$$

The activation energy is then calculated to be:

$$E_a = 8.31441\text{ J mol}^{-1}\text{ K}^{-1} \frac{\ln\left(\frac{0.0345}{0.0538}\right)}{\left(\frac{1}{773\text{ K}} - \frac{1}{673\text{ K}}\right)} \sim 19,218\text{ J mol}^{-1}$$

Alternatively, the activation energy can be calculated from the slope of the regression line given as Equation 8, which is illustrated in [Figure 4](#):

$$\ln[k] = -\frac{E_a}{R} \left(\frac{1}{T}\right) + b \quad (\text{Eq. 20})$$

The slope is -2741.7 K, which corresponds to an activation energy of $\sim 22,796\text{ J mol}^{-1}$ and is reasonably close to the value based upon the 400 and 500°C data. The expression for the rate constant is given as:

$$\ln[k(\text{min}^{-1})] = -2741.7 \times \left(\frac{1}{T(\text{K})}\right) - 6.9712 \quad R^2 = 0.9887 \quad (\text{Eq. 21})$$

The maximum oxide thickness, X_{max} , also depends upon the absolute temperature, as shown in [Figure 5](#). Equation 10 shows the dependence of the maximum oxide thickness as a function of temperature.

$$\ln[X_{max}(\text{nm})] = -6537.9 \times \left(\frac{1}{T(\text{K})}\right) + 12.054 \quad R^2 = 0.9851 \quad (\text{Eq. 22})$$

The apparent maximum oxide thickness, X_{max} , also appears to vary with temperature as shown in Figure 5. In combination, Equations 13, 21 and 22 comprise a model for the DOX of titanium. The model presented here is a simple empirical equation that fits the published data. In the future, better mechanistic models should be developed for the oxidation of titanium alloys.

Table 1. Data Taken from Reference

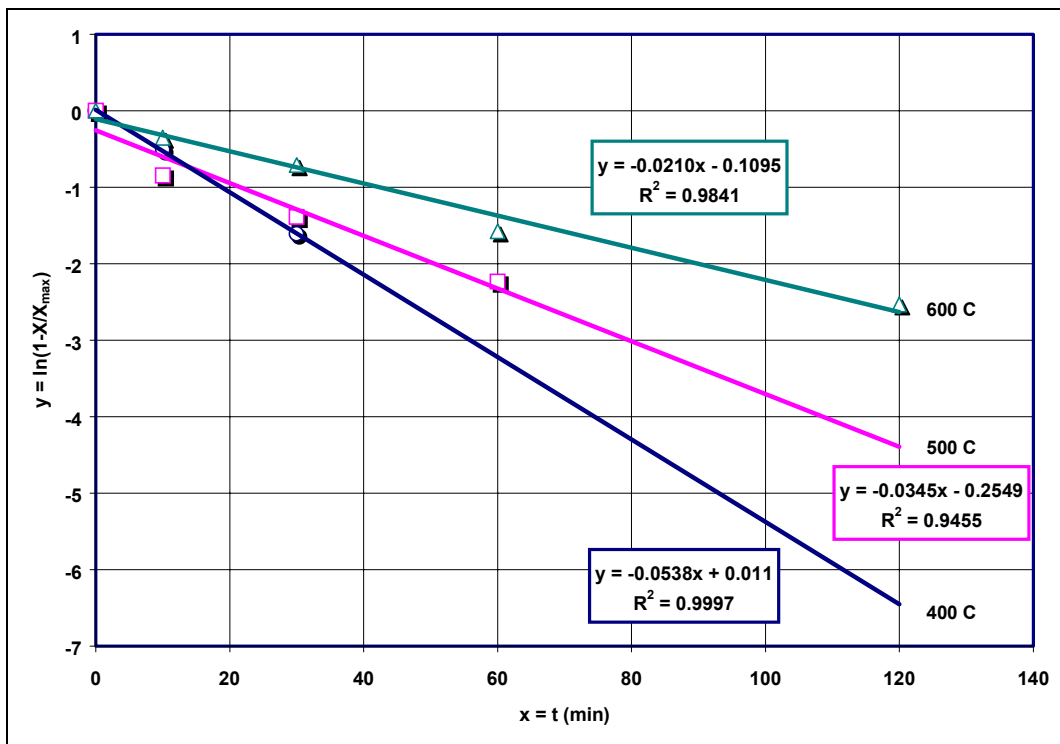
| | 400°C | 500°C | 600°C | 400°C | 500°C | 600°C |
|------|--------|--------|--------|--------------------|--------------------|--------------------|
| Time | Oxide | Oxide | Oxide | Oxide | Oxide | Oxide |
| min | nm | nm | nm | $\ln(1-X/X_{max})$ | $\ln(1-X/X_{max})$ | $\ln(1-X/X_{max})$ |
| 0 | 0.000 | 0.000 | 0.000 | 0 | 0 | 0 |
| 10 | 4.444 | 17.778 | 31.111 | -0.510832291 | -0.84730262 | -0.351397887 |
| 30 | 8.889 | 23.333 | 53.333 | -1.609477914 | -1.38630508 | -0.709147522 |
| 60 | 11.111 | 27.778 | 83.333 | | -2.23362198 | -1.578185369 |
| 120 | 11.111 | 31.111 | 96.667 | | | -2.533696814 |

DTN: LL000201305924.120

Table 2. Parameters in Dry Oxidation Rate Equation Determined by Regression Analysis

| T (°C) | X_{max} (nm) | K (min^{-1}) | $k \times t_0$ | R^2 |
|--------|----------------|-------------------------|----------------|--------|
| 400 | 11.11 | 0.0538 | +0.0110 | 0.9997 |
| 500 | 31.11 | 0.0345 | -0.2549 | 0.9455 |
| 600 | 105 | 0.0210 | -0.1095 | 0.9841 |

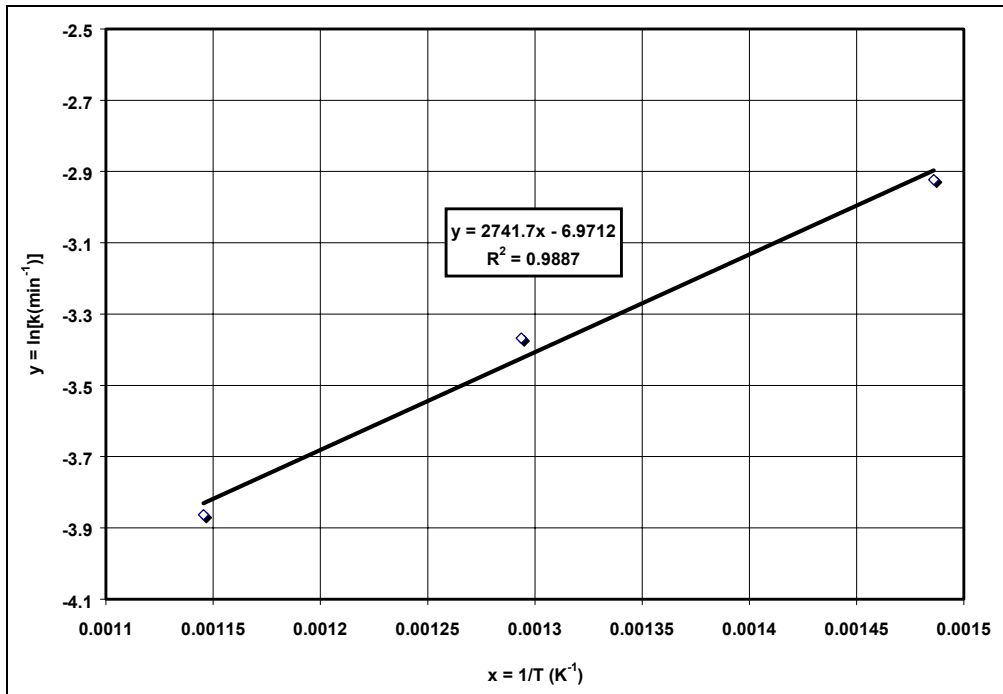
DTN: LL000201405924.121



DTN: LL000201405924.121

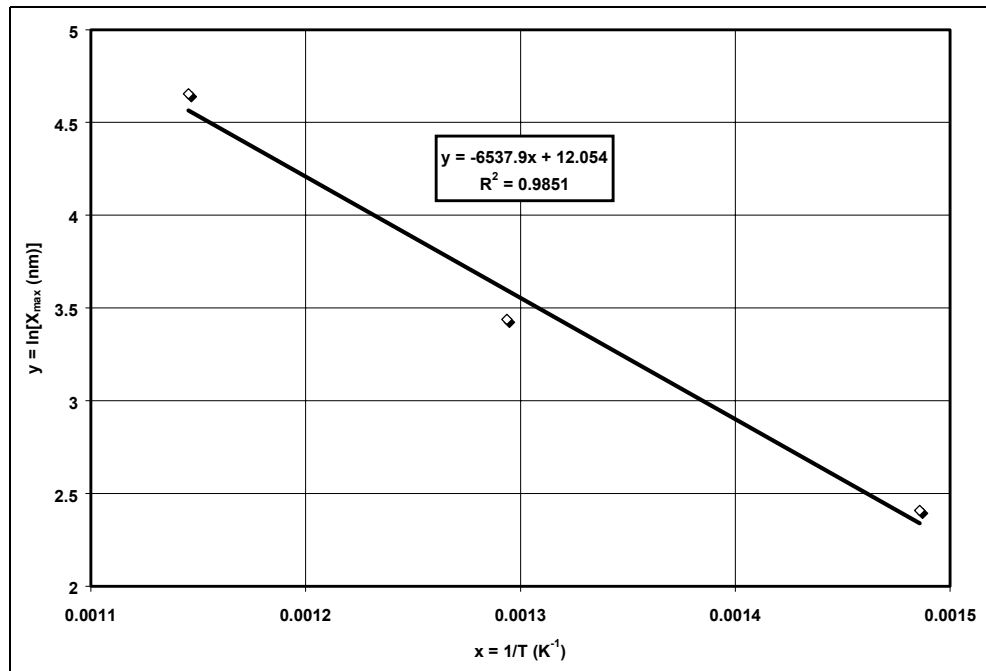
NOTE: Pohlman (1987, p. 685, Fig. 25)

Figure 3. Regression Analysis of Dry Oxidation Rate Data for Titanium



DTN: LL000201405924.121

Figure 4. Determination of Rate Constant as Function of Temperature



DTN: LL000201405924.121

Figure 5. Determination of Maximum Oxide Thickness as Function of Temperature

6.2 HUMID AIR CORROSION

HAC is assumed to occur above a threshold RH, provided that there is no dripping:

$$RH \geq RH_{critical} \quad (\text{Eq. 23})$$

The threshold RH for HAC ($RH_{critical}$) is obeys Equation 1, which is based upon the AMR entitled *Environment on the Surface of Drip Shield and Waste Package Outer Barrier* (CRWMS M&O 2000a). This threshold exists because water absorption by salts precipitated on the WP surface depends on RH.

Despite significant experimental work at LLNL, there continues to be significant uncertainty in the threshold RH for HAC and APC. It may be reasonable to consider HAC at an RH below that predicted with Equation 1. The approximate number of water monolayers on typical metal surfaces as a function of RH has been published (Leygraf 1995) and is repeated in Table 1 of the companion AMR on GC and LC of the WPOB (CRWMS M&O 2000c). Based upon this data, it is believed that two monolayers of water can exist on a metal surface at only 40% RH. It is assumed that at least two monolayers of water are required for HAC or APC. True APC with dissolved ions is difficult to imagine with a single monolayer. However, it is generally believed that at least 70% RH is required on such surfaces for significant electrochemically activity. According to the ASM Handbook (Pohlman 1987), damp corrosion requires moisture in the atmosphere and increases in aggressiveness with the moisture content. When the humidity exceeds a critical value, which is around 70% RH, an invisible thin film of moisture will form on the surface of the metal, providing an electrolyte for current transfer. The critical value depends on surface conditions such as cleanliness, corrosion product buildup, or the presence of salts or other contaminants that are hygroscopic and can absorb water at lower relative humidities. A RH of only 40% might not be enough to cause any corrosion, even with the existence of two monolayers of water on the surface. As pointed out by Gdowski (CRWMS M&O 2000a), observed deliquescence points cover a very broad range of RH. The deliquescence point of NaOH is 1.63% RH at 75°C, while that of K₂SO₄ is 97.59% RH at 20°C. It is assumed that the uncertainty in $RH_{critical}$ can be represented by a triangular distribution. The triangular distribution is described in the companion AMR on the WPOB (CRWMS M&O 2000c). The value at the 50th percentile is represented by Equation 1. Values at the 0th and 100th percentiles are assumed to be 1.63 and 97.59%, respectively.

HAC is treated as uniform GC. The distributions of GC rates given in Sections 6.5.2 and 6.5.4 are based upon Ti Grade 16 samples exposed to both vapor and liquid phase environments. There did not seem to be any significant difference between rates from the two types of exposure. Therefore, all data was combined into a single distribution and used as the basis for estimating GC rates for both HAC and APC, as well as the corresponding variability and uncertainty. It will also be assumed that the corrosion rate is constant and does not decay with time. This provides for conservatism.

HAC occurs uniformly over each WAPDEG patch, which is comparable in size to that of a LTCTF sample with generic weight-loss geometry. Effects of backfill are not considered in the

treatment of HAC threshold and rate. This is consistent with results for artificial titanium crevices exposed in the LTCTF for 12 months.

6.3 AQUEOUS PHASE CORROSION

At a given surface temperature, the existence of liquid-phase water on the WP depends upon the presence of a salt and mineral deposit. In the presence of such a deposit, a liquid-phase can be established at a higher temperature than otherwise possible. In the model discussed here, two conditions must be met for APC: dripping water and RH above the $RH_{critical}$ induced by the salt deposit at the temperature of the WP surface.

$$RH \geq RH_{critical} \quad (\text{Eq. 24})$$

This threshold RH for HAC ($RH_{critical}$) obeys Equation 1, which is based upon the deliquescence point of NaNO_3 salt as discussed in the AMR entitled *Environment on the Surface of Drip Shield and Waste Package Outer Barrier* by Gdowski (CRWMS M&O 2000a). As discussed in Section 6.2, the uncertainty in $RH_{critical}$ can be represented by a triangular distribution. The composition of the electrolyte formed on the WP surface is conservatively assumed to be that of SCW below 100°C and that of SSW above 100°C.

APC is treated as uniform GC. The distributions of GC rates given in Sections 6.5.2 and 6.5.4 are based upon Ti Grade 16 samples exposed to both vapor and liquid phase environments. There did not seem to be any significant difference between rates from the two types of exposure. Therefore, all data was combined into a single distribution and used as the basis for estimating GC rates for both HAC and APC, as well as the corresponding variability and uncertainty. It is conservatively assumed that the corrosion rate is constant and does not decay with time.

General APC occurs uniformly over each WAPDEG patch, which is comparable in size to that of a LTCTF sample with generic weight-loss geometry. Effects of backfill are not considered in the treatment of HAC threshold and rate. This is consistent with results for artificial titanium crevices exposed in the LTCTF for 12 months.

6.4 LOCALIZED CORROSION

6.4.1 Threshold Potential for Ti Grade 7

The LC model for the titanium DS assumes that localized attack occurs if the open circuit corrosion potential (E_{corr}) exceeds the threshold potential for breakdown of the passive film ($E_{critical}$):

$$E_{corr} \geq E_{critical} \quad (\text{Eq. 25})$$

6.4.2 Cyclic Polarization in Synthetic Concentrated J-13 Well Waters

The YMP has used CP to determine threshold potentials for titanium alloys in various test media relevant to the environment expected in the repository. Relevant test environments include

SDW, SCW, and SAW at 30, 60, and 90°C, as well as SSW at 100 and 120°C. The compositions of these test media are based upon the work at LLNL (Gdowski UCRL-ID-132287; UCRL-ID-132286; UCRL-ID-132285). The SSW composition has been recently developed (CRWMS M&O 2000c) and is documented in a companion AMR on GC and LC of the WPOB (CRWMS M&O 2000c). These test media are described in Table 3 below.

Table 3. Composition of Standard Test Media Based upon J-13 Well Water

| Ion | SDW (mg/L ⁻¹) | SCW (mg/L ⁻¹) | SAW (mg/L ⁻¹) | SSW (mg/L ⁻¹) |
|--------------------------------|------------------------------|------------------------------|------------------------------|------------------------------|
| K ⁺¹ | 3.400E+01 | 3.400E+03 | 3.400E+03 | 1.416E+05 |
| Na ⁺¹ | 4.090E+02 | 4.090E+04 | 4.090E+04 | 4.870E+04 |
| Mg ⁺² | 1.000E+00 | 1.000E+00 | 1.000E+03 | 0.000E+00 |
| Ca ⁺² | 5.000E-01 | 1.000E+00 | 1.000E+03 | 0.000E+00 |
| F ⁻¹ | 1.400E+01 | 1.400E+03 | 0.000E+00 | 0.000E+00 |
| Cl ⁻¹ | 6.700E+01 | 6.700E+03 | 6.700E+03 | 1.284E+05 |
| NO ₃ ⁻¹ | 6.400E+01 | 6.400E+03 | 6.400E+03 | 1.310E+06 |
| SO ₄ ⁻² | 1.670E+02 | 1.670E+04 | 1.670E+04 | 0.000E+00 |
| HCO ₃ ⁻¹ | 9.470E+02 | 7.000E+04 | 0.000E+00 | 0.000E+00 |
| Si | 27 (60°C), 49 (90°C) | 27 (60°C), 49 (90°C) | 27 (60°C), 49 (90°C) | 0.000E+00 |
| PH | 8.100E+00 | 8.100E+00 | 2.700E+00 | 7.000E+00 |

NOTE: CRWMS M&O (2000a)

CP measurements have been based on ASTM G 5-87 1989. Representative CP curves are shown in Figures 6 through 10 of this report. Measured values of E_{corr} and $E_{critical}$ are Summarized in Tables 4a and 4b. The reader should also note the relevance of other procedures such as ASTM G 3-89 1997 and G 61-86 1997. Any necessary deviations are noted in the corresponding Scientific Notebooks (SNs). For example, the procedure calls for sulfuric acid, whereas simulated Yucca Mountain waters are used here. Furthermore, unlike the procedure, the electrolytes used here were fully aerated. In general, complete passivity (no passive film breakdown) is shown by these curves between the corrosion potential and the point defined as Threshold Potential 1, which is in the potential range where oxygen evolution is defined by a large excursion in anodic current.

Scully et al. (1999) define the threshold potential for crevice corrosion of Alloy 22 as the point during the scan of electrochemical potential in the forward direction where the current density increases to a level of 10^{-6} to 10^{-5} A cm⁻². Gruss et al. (1998, Table 2) define the repassivation potential as the point where the current density drops to 10^{-6} to 10^{-7} A cm⁻², which is comparable to the definition of Repassivation Potential 3.

6.4.3 Potential Versus Temperature Correlation for Various Test Media

Values of corrosion and threshold potentials have been correlated as a function of temperature for the conditions of interest and are summarized in Tables 4a and 4b. These data have been correlated with temperature as shown in Figures 11 through 14. In general, it has been found that these potential verses temperature data can be represented by the following simple regression equation:

$$y = b_0 + b_1x + b_2x^2 \quad (\text{Eq. 26})$$

where y is either the corrosion or threshold potential (mV vs. Ag/AgCl), and x is the temperature ($^{\circ}\text{C}$). The threshold potential is interpreted as $E_{critical}$, though it may only be a lower bound for $E_{critical}$. The correlations for E_{corr} and $E_{critical}$ are summarized in Table 5.

It is assumed that the specifications for the DS material include allowable values for E_{corr} and $E_{critical}$. Acceptance of the material requires that: (1) the measured value of E_{corr} in a particular environment cannot exceed the value calculated with the corresponding correlation in Table 5 by more than 500 mV and (2) the measured value of $E_{critical}$ in a particular environment cannot be less than the value calculated with the corresponding correlation in Table 5 by more than 500 mV. This is discussed in more detail in Section 6.10, as well as in the following paragraph.

The correlations given in Table 5 were used to calculate the values of E_{corr} and $E_{critical}$ shown in Table 6 for SDW, SCW, SAW, and SSW. Table 6 shows the difference between E_{crit} and E_{corr} (column heading *Diff.*) is never less than 995 mV between 20 and 150 $^{\circ}\text{C}$. Therefore, implementation of the potential-based specification will prevent the use of heats of material that would be prone to passive film instability or LC. The cost of such performance would be associated with the quantity of rejected material, which in the case of titanium would be minimal. The specification can be changed to allow more material to be accepted but with greater risk of LC.

In an ideal case, the crevice corrosion temperature can be estimated from the intersection of the lines representing the corrosion and threshold potentials at elevated temperature. To force crevice corrosion to occur in the model, E_{corr} and $E_{critical}$ can simply be equated over temperature ranges of uncertainty (90 to 120 $^{\circ}\text{C}$). Additional data is needed to fill this void. However, none of the CP curves indicate enough hysteresis to justify any possibility of crevice corrosion.

For the time being, it is expected that the entire external surface of the DS has formed a crevice with either rocks or backfill. The pH in this crevice region may be lower than that of the NFE, though no significant LC has been observed in artificial titanium crevices exposed in the LTCTF for 12 months. Therefore, SAW water chemistry with a pH of approximately 2.7 is assumed. The potential verses temperature correlation for SAW should be used to determine whether or not the threshold for LC has been exceeded in this crevice region.

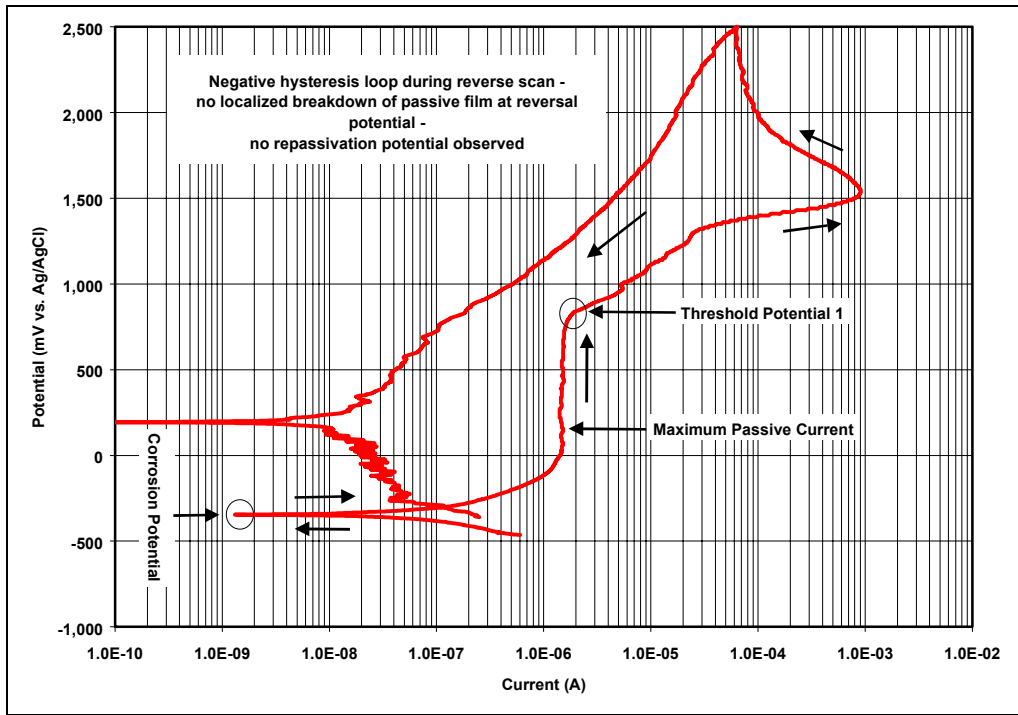


Figure 6. Titanium Grade 7 in SSW at 120°C (NEA031s)

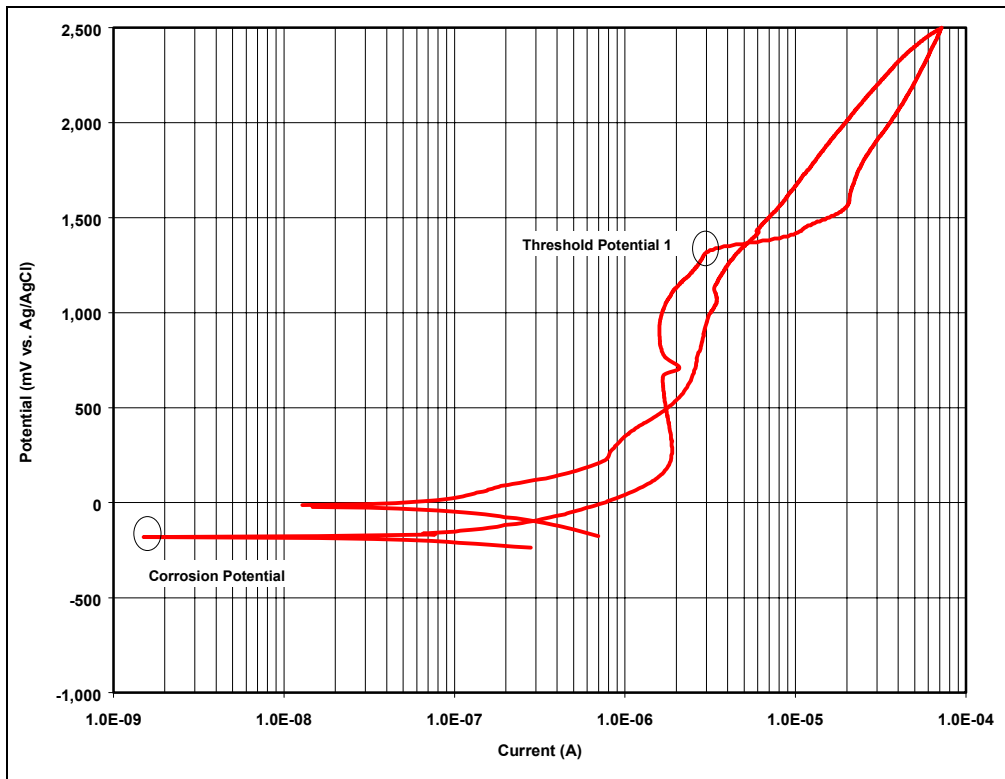


Figure 7. Titanium Grade 7 in SAW at 90°C (NEA025)

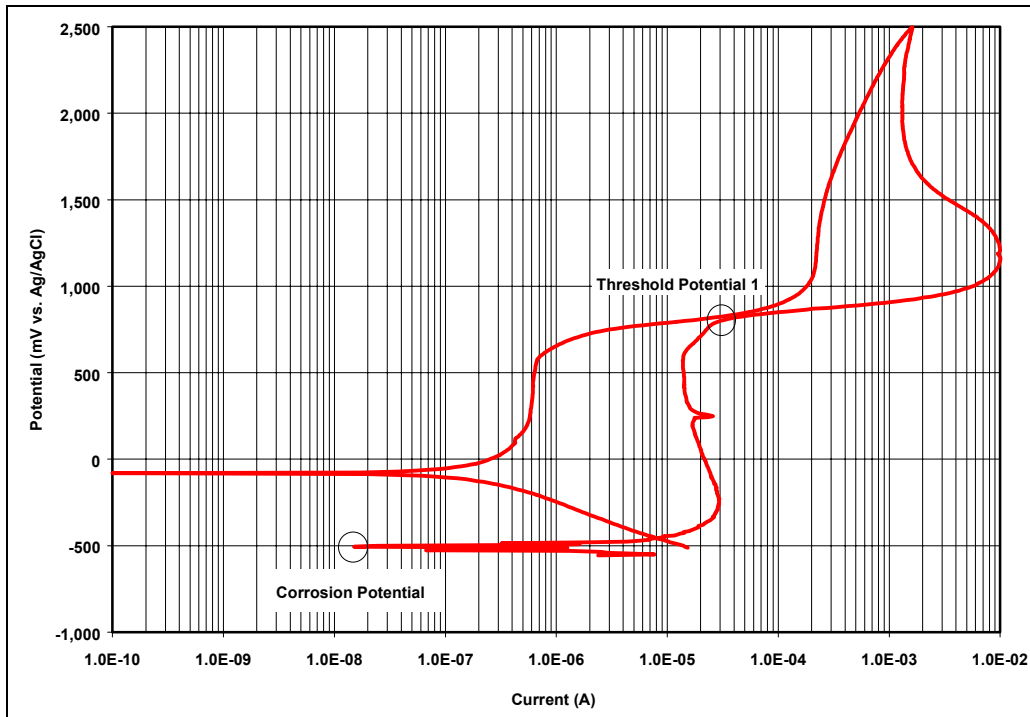


Figure 8. Titanium Grade 7 in SCW at 90°C (NEA029)

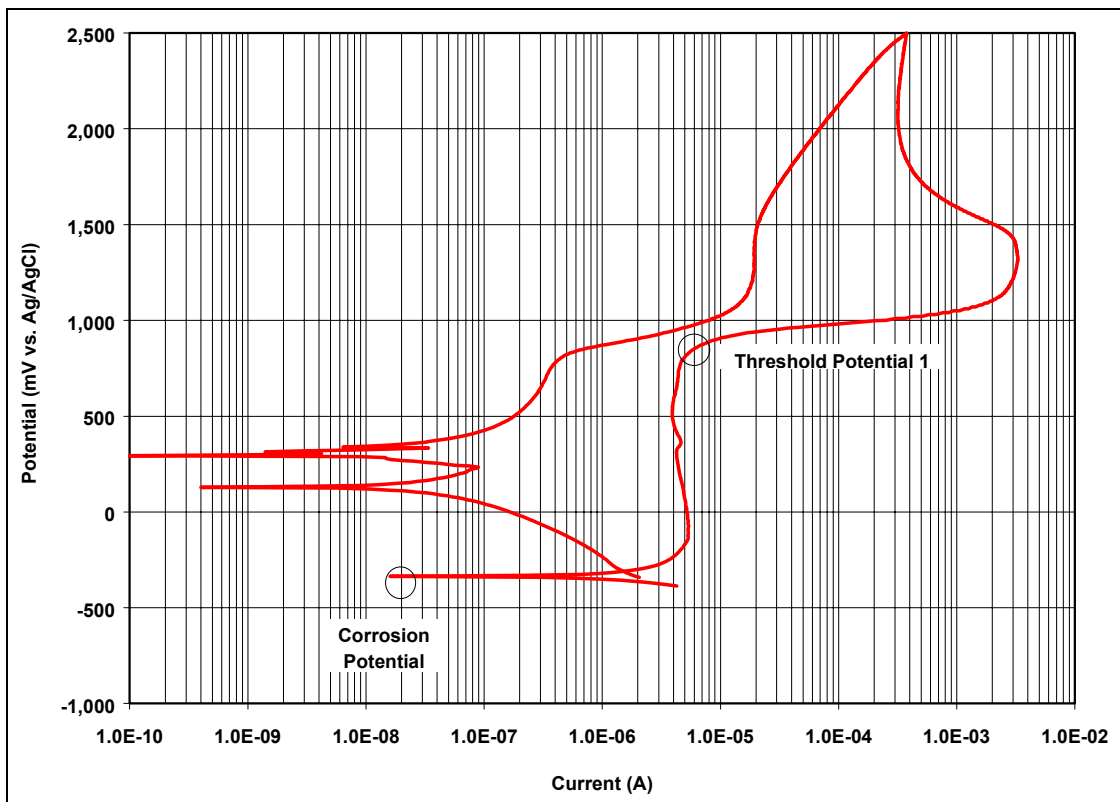


Figure 9. Titanium Grade 7 in SCW at 60°C (NEA019)

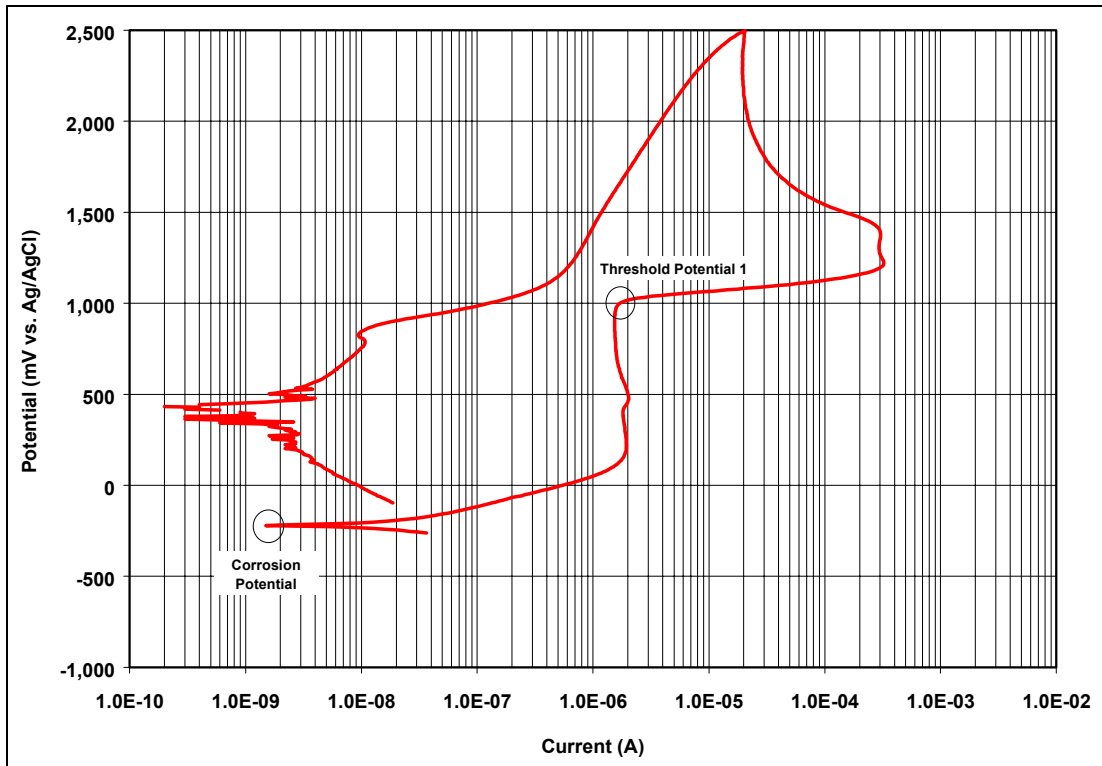


Figure 10. Titanium Grade 7 in SCW at 90°C (NEA003)

Table 4a. Summary of Cyclic Polarization Data for Titanium Grade 7 in Repository-Relevant Conditions (SDW)

| Sample ID | Electrolyte | Temp. (°C) | Corrosion Potential (mV) | Threshold Potential 1 (mV) | Passive Current (amps) | Repassivation Potential 1 (mV) | Repassivation Potential 2 (mV) | Repassivation Potential 3 (mV) | CP Curve (Type) |
|-----------|-------------|------------|--------------------------|----------------------------|------------------------|--------------------------------|--------------------------------|--------------------------------|-----------------|
| NEA002 | SDW | 30 | -145 | 1070 | 8.71E-07 | no breakdown | no breakdown | no breakdown | Type 4 |
| NEA020 | SDW | 60 | -212 | 947 | 1.07E-06 | no breakdown | no breakdown | no breakdown | Type 4 |
| NEA033 | SDW | 90 | -305 | 808 | 1.05E-08 | no breakdown | no breakdown | no breakdown | Type 4 |
| NEA001 | SDW | 30 | -99 | 1000 | 1.15E-06 | no breakdown | no breakdown | no breakdown | Type 4 |
| NEA034 | SDW | 90 | -305 | 752 | 1.32E-07 | no breakdown | no breakdown | no breakdown | Type 4 |
| NEA011 | SDW | 30 | -125 | 1030 | 9.33E-07 | no breakdown | no breakdown | no breakdown | Type 4 |
| NEA022 | SDW | 60 | -114 | 912 | 1.95E-06 | no breakdown | no breakdown | no breakdown | Type 4 |
| NEA023 | SDW | 60 | -214 | 874 | 1.07E-06 | no breakdown | no breakdown | no breakdown | Type 4 |
| NEA005 | SCW | 30 | -37 | 958 | 3.89E-06 | no breakdown | no breakdown | no breakdown | Type 4 |
| NEA017 | SCW | 60 | -331 | 880 | 5.25E-06 | no breakdown | no breakdown | no breakdown | Type 4 |
| NEA028 | SCW | 90 | -480 | 849 | 1.29E-05 | 762 | 798 | breakdown | Type 5 |
| NEA004 | SCW | 30 | -187 | 968 | 2.63E-06 | no breakdown | no breakdown | no breakdown | Type 4 |
| NEA018 | SCW | 60 | -364 | 796 | 6.17E-06 | no breakdown | no breakdown | no breakdown | Type 4 |
| NEA029 | SCW | 90 | -506 | 654 | 2.95E-05 | 752 | 782 | breakdown | Type 5 |
| NEA003 | SCW | 30 | -233 | 1020 | 1.91E-06 | no breakdown | no breakdown | no breakdown | Type 4 |
| NEA019 | SCW | 60 | -351 | 849 | 5.50E-06 | no breakdown | no breakdown | no breakdown | Type 4 |
| NEA030 | SCW | 90 | -516 | 772 | 1.32E-06 | 798 | 808 | breakdown | Type 5 |

Table 4b. Summary of Cyclic Polarization Data for Titanium Grade 7 in Repository-Relevant Conditions (SAW)

| Sample ID | Electrolyte | Temp. (°C) | Corrosion Potential (mV) | Threshold Potential 1 (mV) | Passive Current (amps) | Repassivation Potential 1 (mV) | Repassivation Potential 2 (mV) | Repassivation Potential 3 (mV) | CP Curve (Type) |
|-----------|-------------|------------|--------------------------|----------------------------|------------------------|--------------------------------|--------------------------------|--------------------------------|-----------------|
| NEA010 | SAW | 30 | -153 | 1450 | 2.40E-06 | no breakdown | no breakdown | no breakdown | Type 4 |
| NEA012 | SAW | 30 | -187 | 1430 | 1.48E-06 | no breakdown | no breakdown | no breakdown | Type 4 |
| NEA013 | SAW | 60 | -99 | 1390 | 1.86E-06 | no breakdown | no breakdown | no breakdown | Type 4 |
| NEA024 | SAW | 90 | -187 | 1300 | 1.55E-06 | no breakdown | no breakdown | no breakdown | Type 4 |
| NEA009 | SAW | 30 | -284 | 1420 | 2.69E-06 | no breakdown | no breakdown | no breakdown | Type 4 |
| NEA014 | SAW | 60 | -125 | 1420 | 1.86E-06 | no breakdown | no breakdown | no breakdown | Type 4 |
| NEA025 | SAW | 90 | -187 | 1340 | 1.91E-06 | no breakdown | no breakdown | no breakdown | Type 4 |
| NEA007 | SAW | 30 | -176 | 1440 | 1.35E-06 | no breakdown | no breakdown | no breakdown | Type 4 |
| NEA008 | SAW | 30 | -145 | 1230 | 1.62E-06 | no breakdown | no breakdown | no breakdown | Type 4 |
| NEA026 | SAW | 90 | -176 | 1330 | 1.95E-06 | no breakdown | no breakdown | no breakdown | Type 4 |
| NEA032 | SSW | 100 | -211 | 921 | 3.24E-06 | no breakdown | no breakdown | no breakdown | Type 4 |
| NEA031 | SSW | 120 | -336 | 813 | 1.55E-06 | no breakdown | no breakdown | no breakdown | Type 4 |

NOTE: UI means that the data was uninterpretable and AP means that the CP curve had an active-passive transition. All potentials were measured with a Ag/AgCl reference electrode. One should subtract 197 mV from measured values to convert to the normal hydrogen electrode (NHE) potential scale.

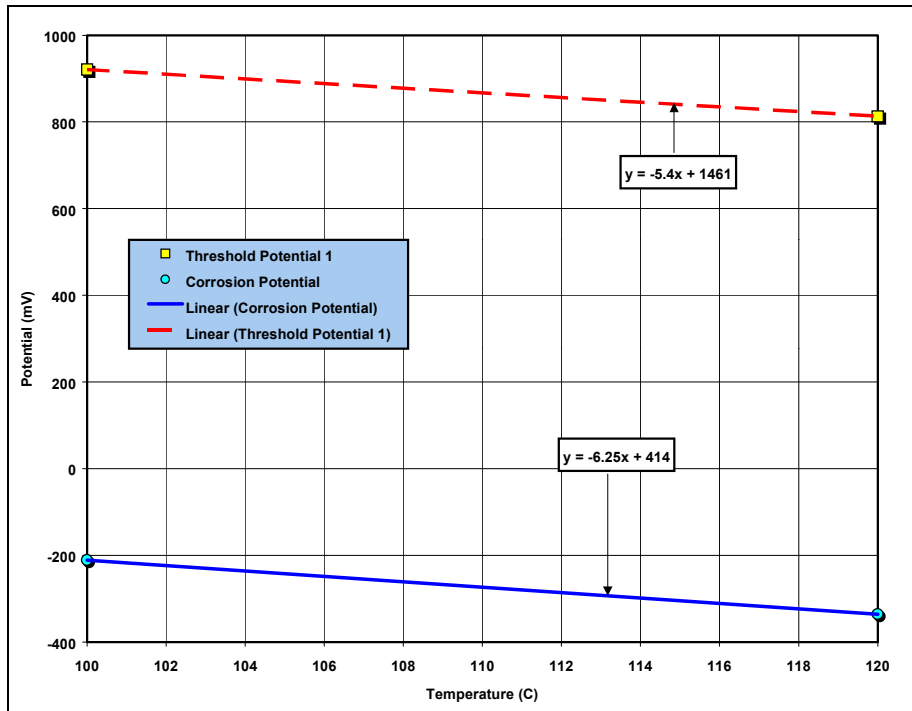


Figure 11. Corrosion and Threshold Potentials of Titanium Grade 7 in SSW (NEA031s)

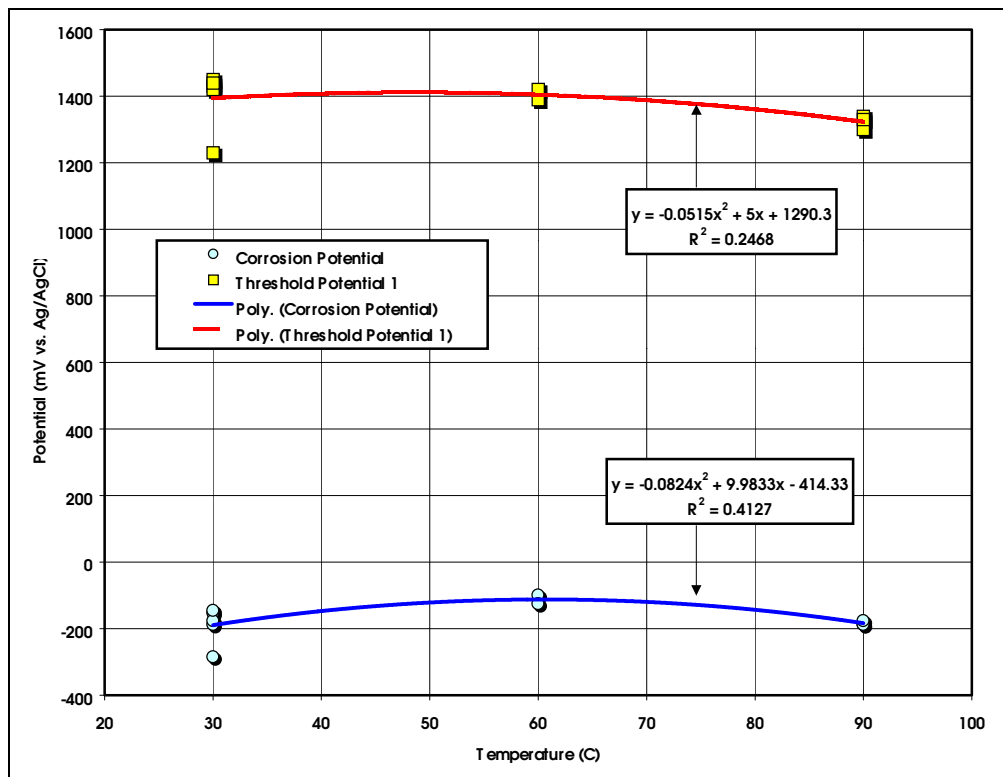


Figure 12. Corrosion and Threshold Potentials for Titanium Grade 7 in SAW

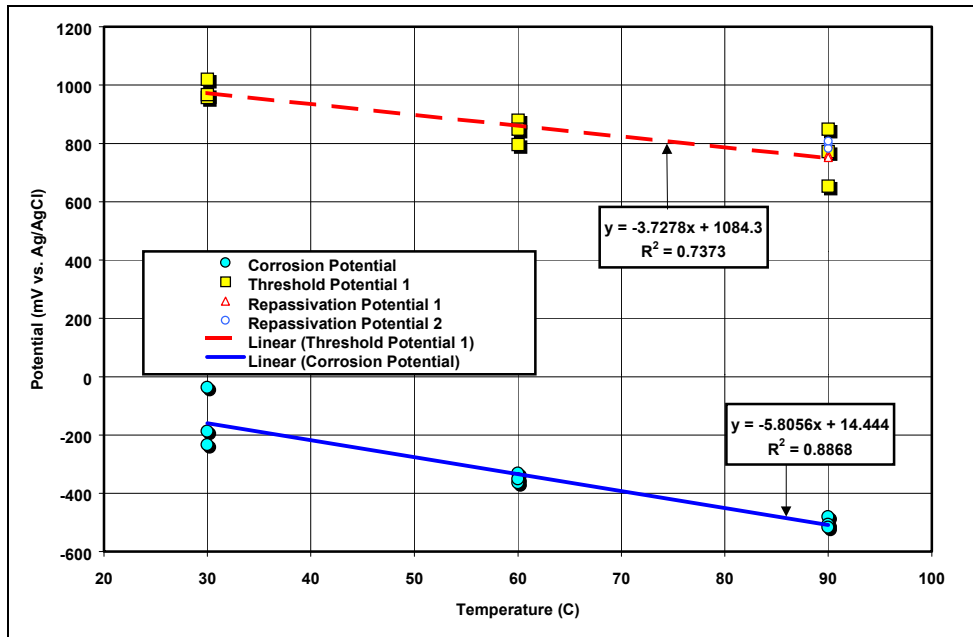


Figure 13. Corrosion and Threshold Potentials for Titanium Grade 7 in SCW

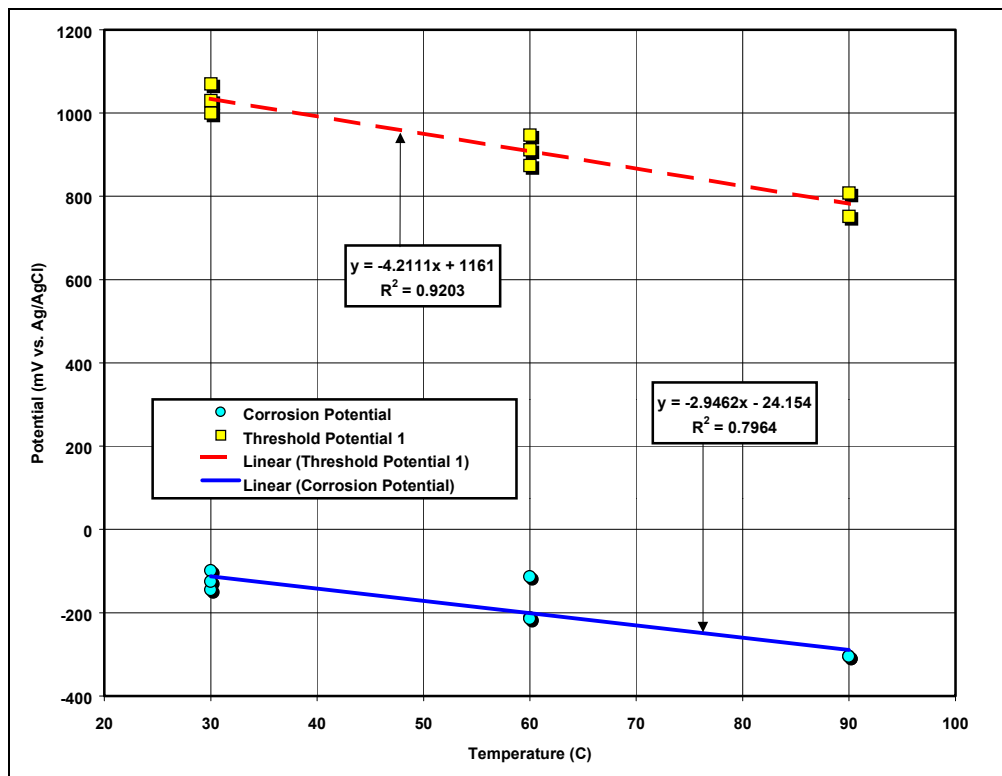


Figure 14. Corrosion and Threshold Potentials for Titanium Grade 7 in SDW

Table 5. Summary of Correlated Corrosion and Threshold Potential Data

| Medium | Potential | Parameter | b_0 | b_1 | b_2 | R^2 |
|--------|-------------|----------------|---------|---------|---------|--------|
| SDW | Corrosion | E_{corr} | -24.154 | -2.9462 | | 0.7964 |
| SDW | Threshold 1 | $E_{critical}$ | 1161 | -4.2111 | | 0.9203 |
| SCW | Corrosion | E_{corr} | 14.444 | -5.8056 | | 0.8868 |
| SCW | Threshold 1 | $E_{critical}$ | 1084.3 | -3.7278 | | 0.7373 |
| SAW | Corrosion | E_{corr} | -414.3 | 9.9833 | -414.33 | 0.4127 |
| SAW | Threshold | $E_{critical}$ | 1290.3 | 5 | -0.0515 | 0.2468 |
| SSW | Corrosion | E_{corr} | 414 | -6.25 | | None |
| SSW | Threshold 1 | $E_{critical}$ | 1461 | -5.4 | | None |

Table 6. Values of E_{corr} and $E_{critical}$ Derived From Correlated Cyclic Polarization Data

| | SDW | SDW | SDW | SCW | SCW | SCW | SAW | SAW | SAW | SSW | SSW | SSW |
|-----|------------|----------------|-------|------------|----------------|-------|------------|----------------|-------|------------|----------------|-------|
| T | E_{corr} | $E_{critical}$ | Diff. |
| °C | mV | mV | mV |
| 20 | -83 | 1077 | 1160 | -102 | 1010 | 1111 | -248 | 1370 | 1617 | 289 | 1353 | 1064 |
| 30 | -113 | 1035 | 1147 | -160 | 972 | 1132 | -189 | 1394 | 1583 | 227 | 1299 | 1073 |
| 40 | -142 | 993 | 1135 | -218 | 935 | 1153 | -147 | 1408 | 1555 | 164 | 1245 | 1081 |
| 50 | -171 | 950 | 1122 | -276 | 898 | 1174 | -121 | 1412 | 1533 | 102 | 1191 | 1090 |
| 60 | -201 | 908 | 1109 | -334 | 861 | 1195 | -112 | 1405 | 1517 | 39 | 1137 | 1098 |
| 70 | -230 | 866 | 1097 | -392 | 823 | 1215 | -119 | 1388 | 1507 | -24 | 1083 | 1107 |
| 80 | -260 | 824 | 1084 | -450 | 786 | 1236 | -143 | 1361 | 1504 | -86 | 1029 | 1115 |
| 90 | -289 | 782 | 1071 | -508 | 749 | 1257 | -183 | 1323 | 1506 | -149 | 975 | 1124 |
| 100 | -319 | 740 | 1059 | -566 | 712 | 1278 | -240 | 1275 | 1515 | -211 | 921 | 1132 |
| 110 | -348 | 698 | 1046 | -624 | 674 | 1298 | -313 | 1217 | 1530 | -274 | 867 | 1141 |
| 120 | -378 | 656 | 1033 | -682 | 637 | 1319 | -403 | 1149 | 1552 | -336 | 813 | 1149 |
| 130 | -407 | 614 | 1021 | -740 | 600 | 1340 | -509 | 1070 | 1579 | -399 | 759 | 1158 |
| 140 | -437 | 571 | 1008 | -798 | 562 | 1361 | -632 | 981 | 1613 | -461 | 705 | 1166 |
| 150 | -466 | 529 | 995 | -856 | 525 | 1382 | -771 | 882 | 1652 | -524 | 651 | 1175 |

6.4.4 Correction of Measured Potential for Junction Potential

It is important to understand the error in the potential measurements due to the junction potential. A correction has been performed based upon the Henderson Equation (Bard and Faulkner 1980). Calculated values of the isothermal junction potentials are summarized in Tables 7 through 11 of the AMR on GC and LC of the WPOB (CRWMS M&O 2000c), which is repeated below at Table 7. The junction potential given in Table 7, E_j , is the potential drop across the Luggin probe. A positive value indicates that the electrochemical potential on the KCl side of the separator (β phase) is greater than the electrochemical potential in the test medium (α phase) adjacent to the Luggin probe. The potential in the test medium can be calculated from the measured value by subtracting E_j . The thermal gradient across the Luggin probe with saturated KCl should produce no significant potential. Filling the Luggin probe with KCl solution is a slight deviation from ASTM Procedure G 5-87 1989, which could lead to introduction of

additional chloride anion into the test medium. However, given the relatively high concentration of chloride already in the test medium, this is not believed to be a significant problem.

Table 7. Summary of Junction Potential Corrections for Cyclic Polarization (Volts)

| T (°C) | SDW | SCW | SAW | SSW |
|--------|-----------|-----------|-----------|------------|
| 30 | 2.716E-03 | 1.188E-03 | 6.019E-03 | -7.649E-03 |
| 60 | 2.984E-03 | 1.306E-03 | 6.615E-03 | -8.406E-03 |
| 90 | 3.253E-03 | 1.423E-03 | 7.210E-03 | -9.164E-03 |

These corrections are not very large, with the largest being about 9 mV for SCW, and have been justifiably ignored in the present data analysis. The effects of temperature across the Luggin probe are assumed to be negligible.

6.4.5 Prediction of Critical Temperatures for Pitting and Crevice Corrosion

As previously discussed, a threshold temperature (critical temperature) can be used as an alternative to a threshold potential for the initiation of LC. In an ideal case, the critical temperatures for pitting and crevice corrosion can be estimated from the intersection of the lines representing the corrosion and threshold potentials as functions of temperature. This intersection occurs at elevated temperature. The critical temperature for pitting of stainless steel 316L is illustrated by Figures 9 and 10. To force crevice corrosion to occur in the model, E_{corr} and $E_{critical}$ can simply be equated above the critical temperature.

6.5 RATES OF GENERAL AQUEOUS-PHASE CORROSION

LC rates will be assumed if the open circuit corrosion potential (E_{corr}) exceeds the threshold potential ($E_{critical}$). GC rates will be assumed if the threshold potential is not exceeded. GC rates will be estimated with weight-loss data from the LTCTF (Estill 1998). LC rates and failure mode characteristics (e.g., number failure sites and opening size) will be estimated from experimental measurements of crevice corrosion made at LLNL. Since pitting has not been observed in laboratory experiments at LLNL, it will be assumed that the primary mode of LC is crevice corrosion. This APC model will be applied to each patch (spatial element or grid point) in the WAPDEG simulation. To the extent possible, uncertainty will be estimated from available data.

6.5.1 Corrosion Rates Based Upon Electrochemical Measurements

Usually, the corrosion current density, i_{corr} , is determined from the intersection of the anodic and cathodic Tafel lines (Bard and Faulkner, 1980 p. 91, 105-107; Landolt 1995, pp. 6-13). However, this assumes that Butler-Volmer kinetics apply at the interface. Since the titanium surface is passivated with a film of TiO_2 , this may not be true. Furthermore, the relationship between $\log i$ and E in close proximity to the corrosion potential, E_{corr} , does not appear to be perfectly linear. Given these various non-idealities, the local minima in current observed at E_{corr} (circled) can be interpreted as a lower bound for the corrosion current density. The passive

current density, i_{pass} , serves as the upper bound. It is believed that the local minima are relatively close to the corrosion current density, the point at which the anodic and cathodic processes are balanced (conservation of charge).

The corrosion (penetration) rate of an alloy can be calculated from the corrosion current density with the following formula (Jones 1996):

$$\frac{dp}{dt} = \frac{i_{corr}}{\rho_{alloy} n_{alloy} F} \quad (\text{Eq. 27})$$

where p is the penetration depth, t is time, i_{corr} is the corrosion current density, ρ_{alloy} is the density of the alloy, assumed to be approximately 4.54 g cm^{-3} for Ti Grade 7, n_{alloy} is the number of gram equivalents per gram of alloy, and F is Faraday's constant. The value of n_{alloy} can be calculated with the following formula:

$$n_{alloy} = \sum_j \left(\frac{f_j n_j}{a_j} \right) \quad (\text{Eq. 28})$$

where f_j is the mass fraction of the j -th alloying element in the material, n_j are the number of electrons involved in the anodic dissolution process, which is assumed to be congruent, and a_j is the atomic weight of the j -th alloying element. These equations have been used to calculate the penetration rate for Ti Grade 7 as a function of corrosion current density. The results of these calculations are shown in [Tables 8 and 9](#). The penetration rate for this material is linearly proportional to current density and is estimated to be between 11.55 and 11.51 microns per year at one microamp per square centimeter. If the corrosion current is due to oxidation rather than dissolution, the penetration corresponds to the thickness of titanium metal converted to oxide. From [Figures 6 through 10](#), it can be seen that typical values of the corrosion current density range from approximately $10^{-9} \text{ A cm}^{-2}$ to approximately $10^{-8} \text{ A cm}^{-2}$ (10^{-3} to $10^{-2} \mu\text{A cm}^{-2}$). This corresponds to penetration (or oxidation) rates that range from 0.01 to 0.1 microns per year (10 to 100 nanometers per year). This is in reasonable agreement with the rates based on weight loss measurements given in [Section 6.5.2](#).

The lower bound of the corrosion current and the non-equilibrium passive current from CP measurements in SDW, SCW, SAW, and SSW are summarized in [Figures 15 through 18](#). In general, it has been found that the current versus temperature data can be represented by one of the following linear regression equations. The linear and polynomial forms are both represented by:

$$y = b_0 + b_1 x + b_2 x^2 \quad (\text{Eq. 29})$$

The exponential form is represented by:

$$\ln y = \ln b_0 + b_1 \ln x \quad (\text{Eq. 30})$$

where y is the current (A) and x is the temperature ($^{\circ}\text{C}$). This can be rewritten as:

$$y = b_0 \times (x)^{b_1} \quad (\text{Eq. 31})$$

Since the exposed area in these measurements is approximately 0.96 cm^2 , the current density is nearly identical to the current. The coefficients based upon the correlation of data for SDW, SCW, SAW, and SSW are summarized in [Table 10](#). The actual rate at which the titanium corrodes will be somewhere between the value based upon the lower bound of the corrosion current density and the non-equilibrium passive current density. Usually, it is expected that a passive surface corrodes at the passive current density, i_{pass} , under open circuit conditions. Anodic polarization can give higher apparent i_{pass} with non-equilibrium conditions; i.e., the true i_{pass} will be much lower when measured at slower polarization rates. Double layer charging will be observed during potential scans. Such charging will be manifested as a non-equilibrium current density that drops to zero when the potential scan is stopped (equilibrium conditions). Greater charging current is observed at faster scan rates. Such non-equilibrium effects will be confounded with the true passive current density. Anodic polarization is notoriously inaccurate for estimating corrosion rates.

Table 8. Conversion of Current Density to Corrosion (Penetration) Rate

| | | Value at Low f_i | Value at High f_i |
|---------------------------|-----------------------|--------------------|---------------------|
| Faraday Constant | C equiv ⁻¹ | 9.648460E+04 | 9.648460E+04 |
| Assumed Current Density | A cm ⁻² | 1.000000E-06 | 1.000000E-06 |
| Assumed Mass Density | g cm ⁻³ | 4.540000E+00 | 4.540000E+00 |
| Total $(f_j n_j/a_j)/100$ | | 6.233572E-02 | 6.257576E-02 |
| dp/dt | cm s ⁻¹ | 3.662260E-11 | 3.648212E-11 |
| dp/dt | microns per year | 1.154930E+01 | 1.150500E+01 |

Table 9. Conversion of Current Density to Corrosion Rate as Function of Alloy Composition

| | a_j | n_j | n_j | n_j | f_j | f_j | $(f_j n_j/a_j)/100$ | $(f_j n_j/a_j)/100$ |
|-------|-----------|-------|-------|-------|---------|---------|---------------------|---------------------|
| | | | | | Wt. % | Wt. % | | |
| | | Low | High | Calc. | Low | High | Low | High |
| C | 12.011 | 2 | 4 | 4 | 0.000 | 0.080 | 0.000000E+00 | 2.664224E-04 |
| Ni | 58.69 | 2 | 3 | 2 | 0.000 | 0.000 | 0.000000E+00 | 0.000000E+00 |
| Cr | 51.9969 | 3 | 6 | 3 | 0.000 | 0.000 | 0.000000E+00 | 0.000000E+00 |
| Mo | 95.94 | 3 | 6 | 3 | 0.000 | 0.000 | 0.000000E+00 | 0.000000E+00 |
| Fe | 55.847 | 2 | 3 | 2 | 0.300 | 0.000 | 1.074364E-04 | 0.000000E+00 |
| Cu | 63.546 | 1 | 2 | 2 | 0.000 | 0.000 | 0.000000E+00 | 0.000000E+00 |
| P | 30.973762 | 3 | 5 | 5 | 0.000 | 0.000 | 0.000000E+00 | 0.000000E+00 |
| Si | 28.0855 | 4 | 4 | 4 | 0.000 | 0.000 | 0.000000E+00 | 0.000000E+00 |
| S | 32.066 | 2 | 6 | 6 | 0.000 | 0.000 | 0.000000E+00 | 0.000000E+00 |
| Mn | 54.93805 | 2 | 2 | 2 | 0.000 | 0.000 | 0.000000E+00 | 0.000000E+00 |
| W | 183.85 | 2 | 6 | 6 | 0.000 | 0.000 | 0.000000E+00 | 0.000000E+00 |
| Co | 58.9332 | 2 | 3 | 2 | 0.000 | 0.000 | 0.000000E+00 | 0.000000E+00 |
| V | 50.9415 | 2 | 3 | 3 | 0.000 | 0.000 | 0.000000E+00 | 0.000000E+00 |
| Ti | 47.88 | 2 | 3 | 3 | 99.280 | 99.370 | 6.220551E-02 | 6.226190E-02 |
| Pd | 105.42 | 2 | 2 | 2 | 0.120 | 0.250 | 2.276608E-05 | 4.742933E-05 |
| Other | 1 | 0 | 0 | 0 | 0.300 | 0.300 | 0.000000E+00 | 0.000000E+00 |
| Total | | | | | 100.000 | 100.000 | 6.233572E-02 | 6.257576E-02 |

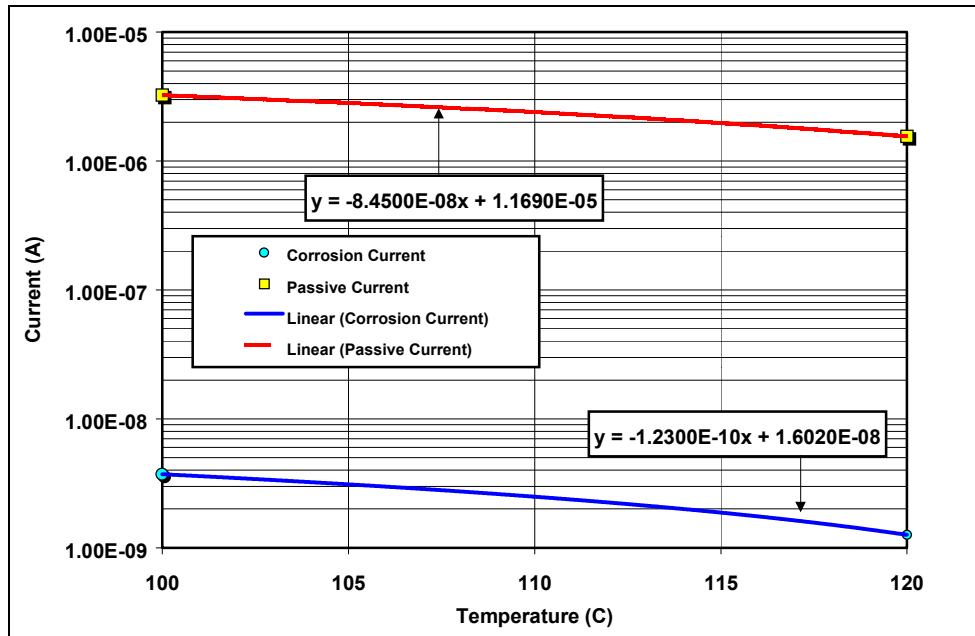


Figure 15. Corrosion and Passive Currents for Titanium Grade 7 in SSW

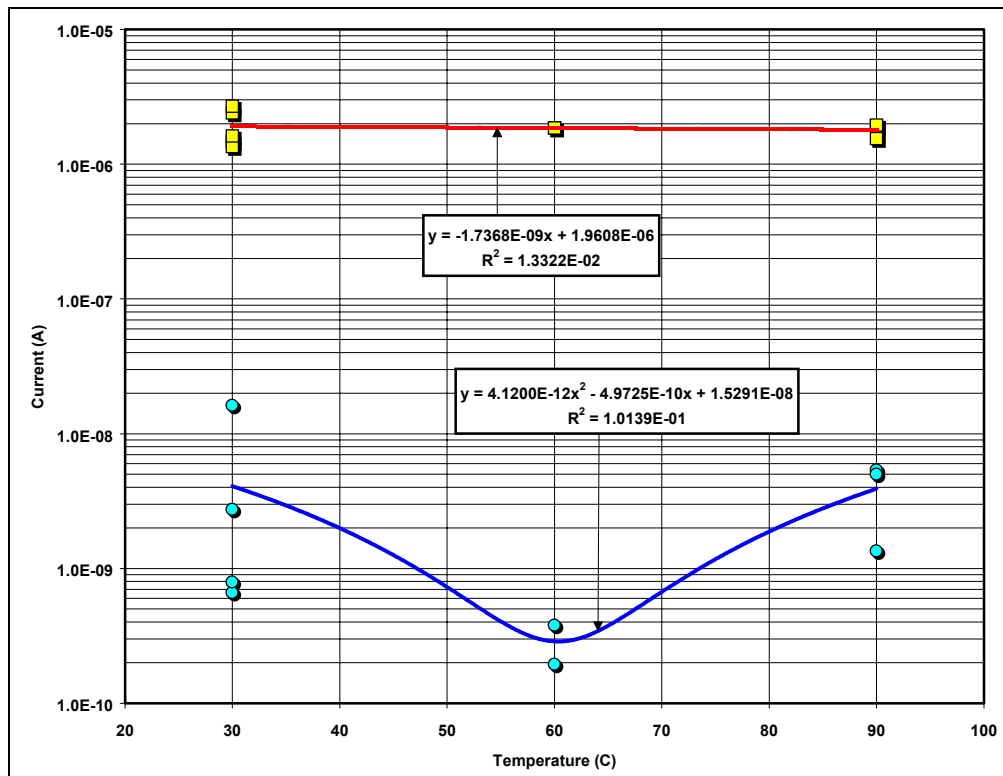


Figure 16. Corrosion and Passive Currents for Titanium Grade 7 in SAW

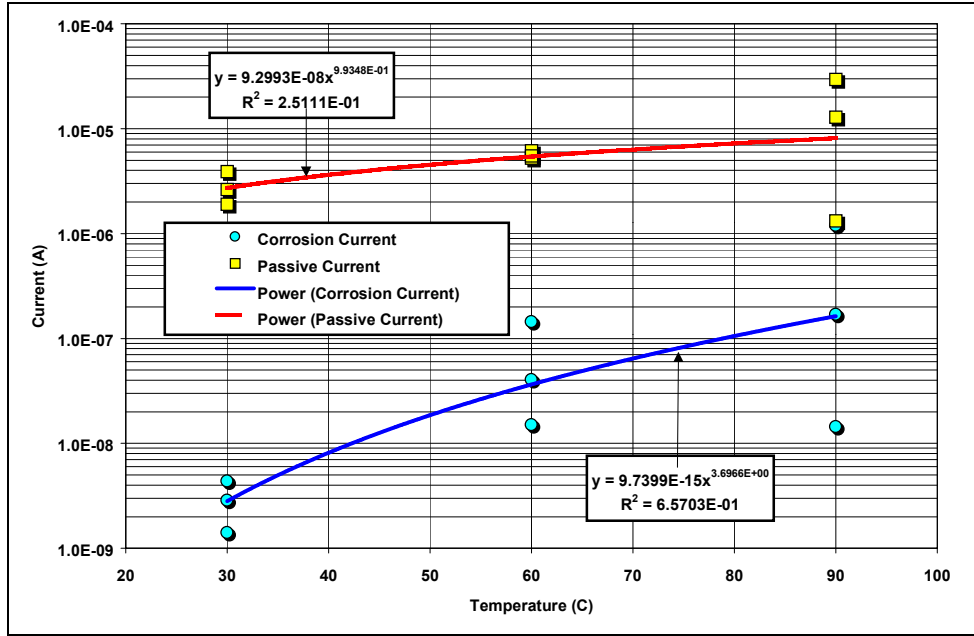


Figure 17. Corrosion and Passive Currents for Titanium Grade 7 in SCW

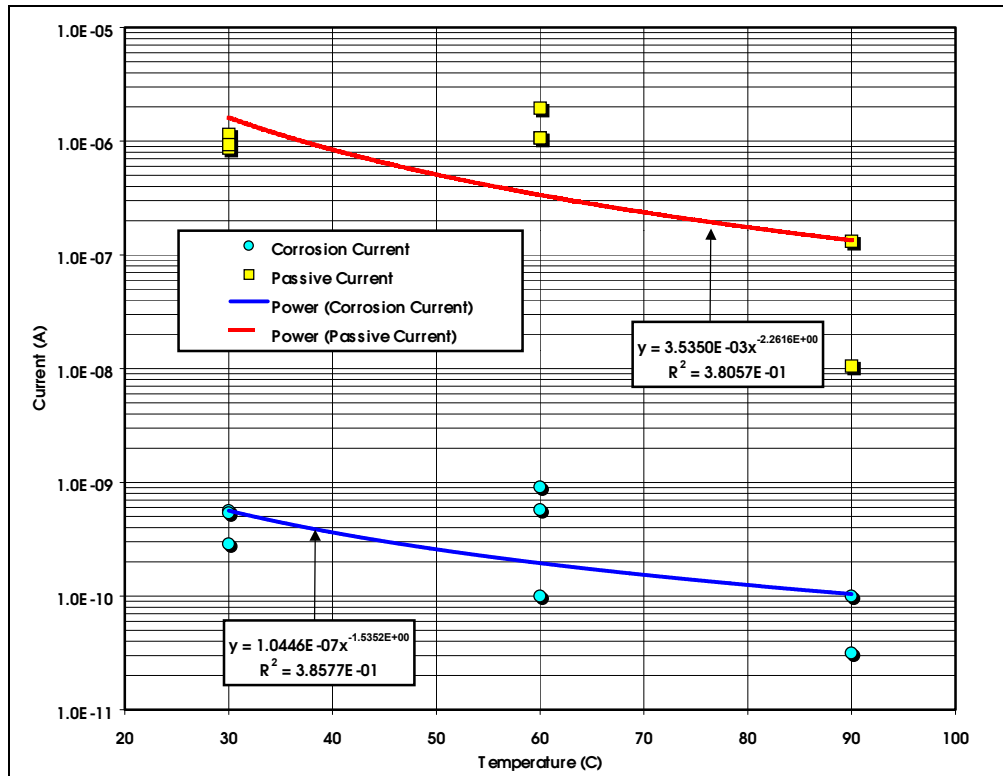


Figure 18. Corrosion and Passive Currents for Titanium Grade 7 in SDW

Table 10. Coefficients for Regression Equations Used to Represent Corrosion and Passive Currents

| Medium | Current | Corresponding Potential | Correlation Type | b_0 | b_1 | b_2 | R^2 |
|--------|-----------|-------------------------|------------------|-------------|-------------|------------|--------|
| SDW | Corrosion | E_{corr} | Power | 1.0446E-07 | -1.5352 | | 0.3858 |
| SDW | Passive | $E_{critical}$ | Power | 3.5350E-03 | -2.2616 | | 0.3806 |
| SCW | Corrosion | E_{corr} | Power | 9.7399E-15 | 3.6966 | | 0.6570 |
| SCW | Passive | $E_{critical}$ | Power | 9.2993E-08 | 0.9935 | | 0.2258 |
| SAW | Corrosion | E_{corr} | Polynomial | 1.5291E-08 | -4.9725E-10 | 4.1200E-12 | 0.1014 |
| SAW | Passive | $E_{critical}$ | Linear | 1.9608E-06 | -1.7368E-09 | | 0.0133 |
| SSW | Corrosion | E_{corr} | Linear | -1.2300E-10 | 1.6020E-08 | | None |
| SSW | Passive | $E_{critical}$ | Linear | 1.1690E-05 | -8.4500E-08 | | None |

6.5.2 Corrosion Rates Based Upon Weight Loss Measurements

The materials for the EDA II design, which includes Ti Grade 7, were selected after the testing program for the LTCTF was established. An alloy similar to Ti Grade 7 was incorporated into the testing program, Ti Grade 16. These two materials appear to have very similar corrosion rates (Gdowski 1997). The primary difference between these two alloys is palladium content. Ti Grade 7 has 0.12 to 0.25 wt.% Pd, whereas Ti Grade 16 has only 0.04 to 0.08 wt.% Pd. The greater Pd content of the Ti Grade 7 may translate into slightly greater resistance to HIC. From the standpoint of GC rates, Ti Grade 16 is assumed to be a good analog for Ti Grade 7. The passive films are believed to be similar.

Testing includes a wide range of plausible generic test media, including SDW, SCW, and SAW. The SCW test medium is three orders-of-magnitude (1000X) more concentrated than J-13 well water and is slightly alkaline (pH~8). The SAW test medium is three orders-of-magnitude (1000X) more concentrated than J-13 well water and is acidic (pH~2.7). Two temperature levels (60 and 90°C) are included in this qualified (Q) testing program. It will be further assumed that all drip shields undergo GC at a constant rate, characterized by the distributions shown in this section and Section 6.5.4. The maximum observed rate, which is much less than 1 micron per year, clearly indicates that the life of the DS will not be limited by GC during a 10,000-year service life. It will also be assumed that the GC rate is constant and does not decay with time. Less conservative corrosion models assume that the rate decays with time.

The LTCTF appears to be the most complete source of corrosion data for relevant titanium alloys (Ti Grade 16) in environments relevant to the proposed HLW repository at Yucca Mountain. This facility is equipped with an array of nearly cubic fiberglass tanks. Each tank has a total volume of ~2000 liters and is filled with ~1000 liters of aqueous test solution. The solution in a particular tank is controlled at either 60 or 90°C, covered with a blanket of air flowing at approximately 150 cm³ min⁻¹ and agitated. The test environments used in the LTCTF are referred to as SDW, SCW, SAW, and SCMW. The descriptions and compositions of three of these solutions are summarized in Table 3. Four generic types of samples—U-bends, crevices, weight loss samples, and galvanic couples—are mounted on insulating racks and placed in the tanks. Approximately half of the samples are submersed, half are in the saturated vapor above the aqueous phase, and a limited number are at the water line. It is important to note that condensed water is present on specimens located in the saturated vapor.

As previously discussed, GC measurements have been based upon ASTM G 1-81 1987. The GC (or penetration) rate of an alloy can be calculated from weight loss data as follows with the following general formula:

$$\text{Corrosion Rate} = \frac{(K \times W)}{(A \times T \times D)} \quad (\text{Eq. 32})$$

where K is a constant, T is the time of exposure in hours, A is the exposed area of the sample in square centimeters, W is the mass loss in grams, and D is the density in grams per cubic centimeter. The value of K used for the LTCTF data was $8.76 \times 10^7 \mu\text{m yr}^{-1} \text{ h cm}^{-1}$ (ASTM G 1-81 1987). This formula for corrosion rate can be rewritten in the following form:

$$\frac{dp}{dt} = \frac{w}{\rho \times t} \frac{1}{[2(a \times b) + 2(b \times c) + 2(a \times c)]} \quad (\text{Eq. 33})$$

where dp/dt is the corrosion rate, w is the mass loss in grams, ρ is the density in grams per cubic centimeter, t is the time of exposure in years, and the quantity in square brackets represents the exposed area of the sample in square centimeters. Without application of any conversion factor, the corrosion rate calculated with this formula has the units of centimeters per year. Multiplication of dp/dt by $10^4 \mu\text{m cm}^{-1}$ yields a corrosion rate with the units of microns per year. The weight loss and dimensional change were measured with electronic instruments calibrated to traceable standards. Since all data was digitally transferred to computer, the possibility of human key-punch error was minimized.

Comparative sample calculations are used to compare the two formulae, (Eqs. 32 and 33). Comparison is necessary to show that the error analysis in Section 6.5.4 applies to the formula given by the ASTM. With specific assumed values, the first formula yields:

$$K = 8.76 \times 10^7 \mu\text{m yr}^{-1} \text{ h cm}^{-1}$$

$$W = 0.0001 \text{ g}$$

$$A = 1.0 \text{ cm}^2$$

$$T = 4320 \text{ h}$$

$$D = 4.54 \text{ g cm}^{-3}$$

$$\text{CorrosionRate} = \frac{(8.76 \times 10^7 \mu\text{m yr}^{-1} \text{ h cm}^{-1})(0.0001 \text{ g})}{(1.0 \text{ cm}^2)(4320 \text{ h})(4.54 \text{ g cm}^{-3})} = 0.45 \mu\text{m yr}^{-1}$$

A calculation with the second formula and the same assumed values give nearly the same result.

$$k = 10^4 \mu\text{m cm}^{-1}$$

$$w = 0.0001 \text{ g}$$

$$2(a \times b) + 2(b \times c) + 2(a \times c) = 1.0 \text{ cm}^2$$

$$t = 0.5 \text{ yr}$$

$$\rho = 4.54 \text{ g cm}^{-3}$$

$$\frac{dp}{dt} = \frac{(10^4 \mu\text{m cm}^{-1})(0.0001 \text{ g})}{(1.0 \text{ cm}^2)(0.5 \text{ yr})(4.54 \text{ g cm}^{-3})} = 0.44 \mu\text{m yr}^{-1}$$

Application of these two formulae give very close but not identical results. The difference is due to round off error in the constants. The second formula is used as the basis of a formal error analysis of GC rates determined from LTCTF data. Note that this formula applies to dissolution but not to oxidation.

All GC rates for Ti Grade 16 based on LTCTF weight loss samples are shown in [Figure 19](#). It appears that these measurements are independent of temperature between 60 and 90°C. Furthermore, the composition of the test medium (SDW, SCW, or SAW) appeared to have little impact on the measurements. With the exception of four outliers, most of the rates plotted in [Figure 19](#) are between -200 and +200 nanometers per year. The median is at approximately zero. Obviously, any negative corrosion rate is an artifact.

The outliers with large negative rates are believed to represent samples where there was significant oxide growth or scale formation.

This analysis only includes Ti Grade 16 samples exposed for 12 months in the LTCTF. As discussed by Estill (1998), the cleaning method employed with the 6-month samples resulted in sufficient metal loss to cause the appearance of high corrosion rates that proved to be artifacts. Very little cleaning was used for the 12-month samples, which may account for the large negative values in [Figures 19 and 20](#) (scale formation).

All GC rates for Ti Grade 16 based on LTCTF crevice samples are shown in [Figure 20](#) (rates based on areas outside of crevice). In this case, it also appears that the measurements are independent of temperature and test medium. Most of the rates plotted in [Figure 20](#) are between -350 and +350 nanometers per year. The median is at approximately zero. The largest measured rate shown in [Figure 20](#), which is less than +350 microns per year, will not lead to failure of the DS during the 10,000 year service life. Based upon these data, it does not appear that the life of the DS will be limited by the GC of Ti Grade 16 (analog of Grade 7) at temperatures less than those involved in the test (90°C) during a period of 10,000 years.

It must be noted that the distributions shown in this section and Section 6.5.4 are based upon LTCTF data at 30, 60, and 90°C. There appeared to be very little temperature dependence over this range. These distributions are being used at slightly higher temperatures, up to the 120°C boiling point of SSW. In the future, additional long-term exposures should be done at 120°C to add confidence to the predictions at higher temperature.

The crevice samples were configured in such a way as to reveal crevice corrosion if it occurred. Since no obvious crevice attack was observed with the samples represented by these figures, it is assumed that all weight loss in the crevice samples was due to GC outside of the crevice region (area underneath washer). However, higher scatter perhaps indicates more variability of corrosion inside the crevice. Corrosion inside is more due to differential aeration and/or minor pH changes within the crevice than LC.

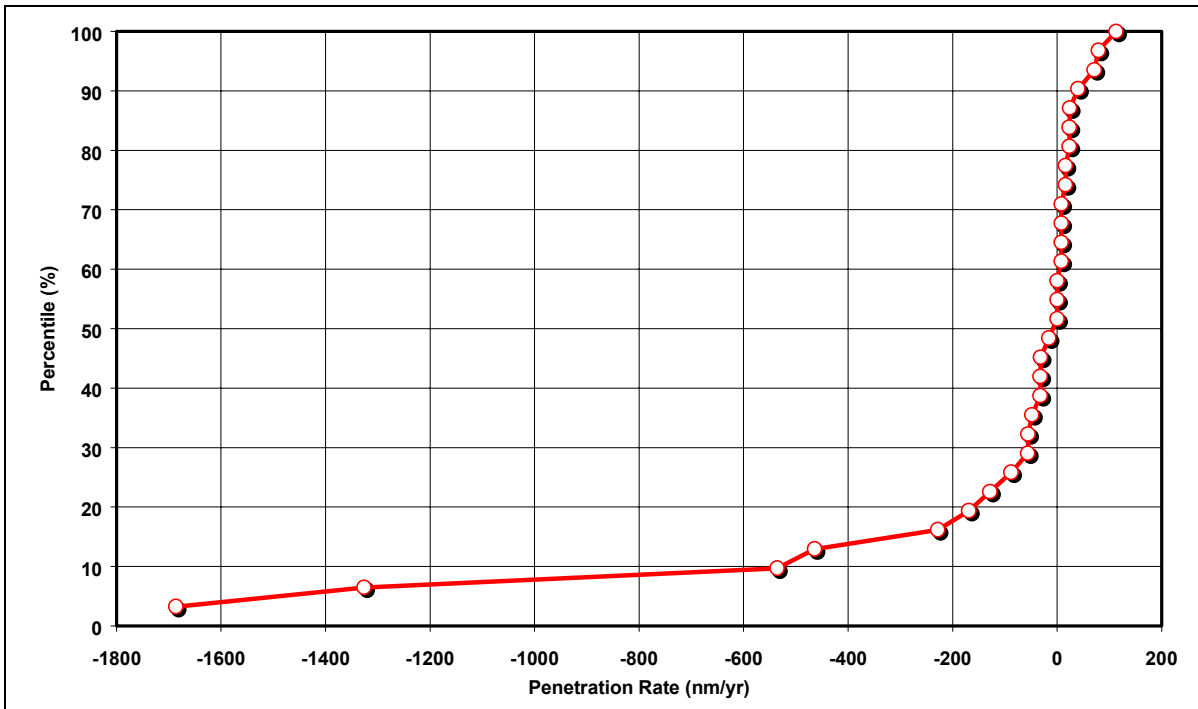


Figure 19. Distribution of General Corrosion Rates of Ti Grade 16: LTCTF 12-Month Wt. Loss Samples

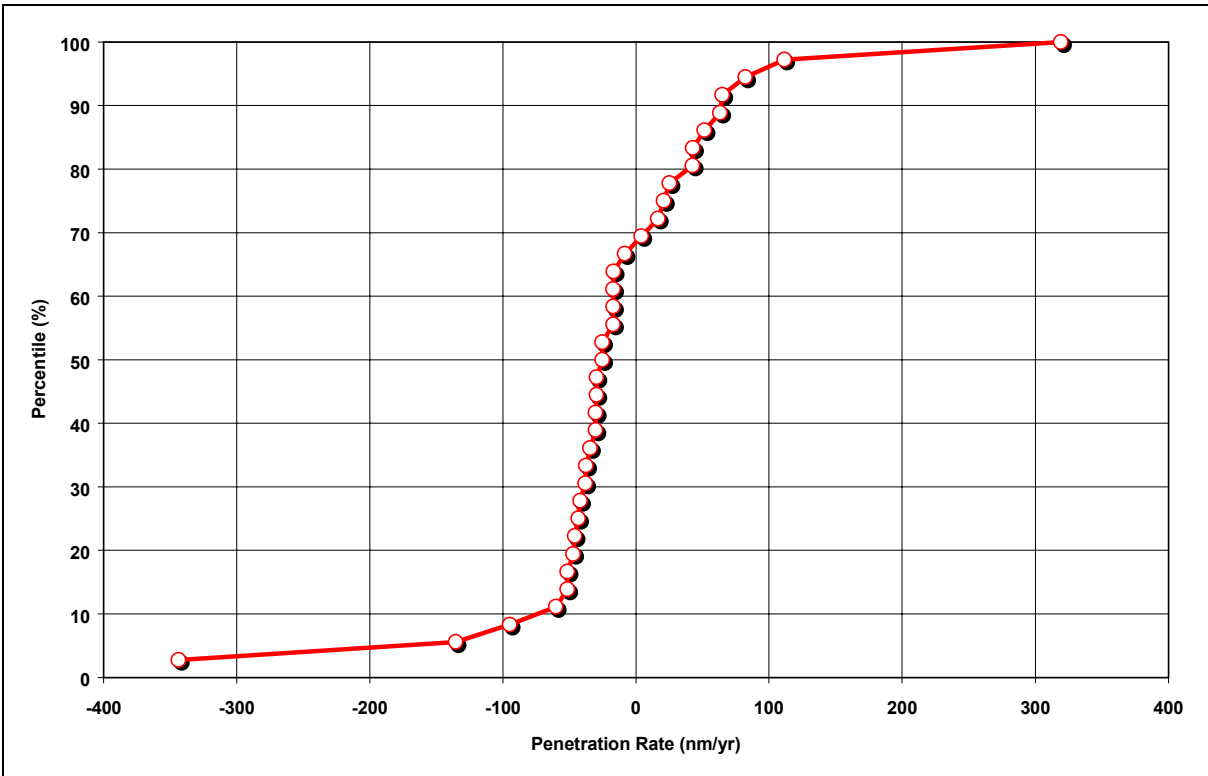


Figure 20. Distribution of General Corrosion Rates of Ti Grade 16: LTCTF 12-Month Crevice Samples

6.5.3 Error Analysis for Weight Loss Measurements

The general method used in the formal error analysis is now presented. Consider the dependent variable y defined by the following generic function:

$$y = f(x_1, x_2, x_3, x_4 \cdots x_n) \quad (6-20)$$

where x_i is the i^{th} independent variable. The total derivative of y is then defined as:

$$dy = \frac{\partial y}{\partial x_1} dx_1 + \frac{\partial y}{\partial x_2} dx_2 + \frac{\partial y}{\partial x_3} dx_3 + \frac{\partial y}{\partial x_4} dx_4 + \cdots + \frac{\partial y}{\partial x_n} dx_n \quad (6-21)$$

Based upon this definition, the maximum error in y can then be defined as:

$$\Delta y = \left| \frac{\partial y}{\partial x_1} \Delta x_1 \right| + \left| \frac{\partial y}{\partial x_2} \Delta x_2 \right| + \left| \frac{\partial y}{\partial x_3} \Delta x_3 \right| + \left| \frac{\partial y}{\partial x_4} \Delta x_4 \right| + \cdots + \left| \frac{\partial y}{\partial x_n} \Delta x_n \right| \quad (6-22)$$

where Δx_i is the error in the i^{th} independent variable. Let the dependent variable y be the GC rate measured in the LTCTF:

$$y = \frac{dp}{dt} = \frac{w}{\rho \times t} \frac{1}{[2(a \times b) + 2(b \times c) + 2(a \times c)]} \quad (6-23)$$

The total derivative of the corrosion rate is:

$$dy = \frac{\partial y}{\partial w} dw + \frac{\partial y}{\partial \rho} d\rho + \frac{\partial y}{\partial t} dt + \frac{\partial y}{\partial a} da + \frac{\partial y}{\partial b} db + \frac{\partial y}{\partial c} dc \quad (6-24)$$

The maximum error in the corrosion rate is:

$$\Delta y = \left| \frac{\partial y}{\partial w} \Delta w \right| + \left| \frac{\partial y}{\partial \rho} \Delta \rho \right| + \left| \frac{\partial y}{\partial t} \Delta t \right| + \left| \frac{\partial y}{\partial a} \Delta a \right| + \left| \frac{\partial y}{\partial b} \Delta b \right| + \left| \frac{\partial y}{\partial c} \Delta c \right| \quad (6-25)$$

The partial derivatives are:

$$\frac{\partial y}{\partial w} = \frac{1}{\rho \times t} \frac{1}{[2(a \times b) + 2(b \times c) + 2(a \times c)]} \quad (6-26)$$

$$\frac{\partial y}{\partial \rho} = \frac{w}{\rho^2 \times t} \frac{1}{[2(a \times b) + 2(b \times c) + 2(a \times c)]} \quad (6-27)$$

$$\frac{\partial y}{\partial t} = \frac{w}{\rho \times t^2} \frac{1}{[2(a \times b) + 2(b \times c) + 2(a \times c)]} \quad (6-28)$$

$$\frac{\partial y}{\partial a} = \frac{w}{\rho \times t} \frac{[2b + 2c]}{[2(a \times b) + 2(b \times c) + 2(a \times c)]^2} \quad (6-29)$$

$$\frac{\partial y}{\partial b} = \frac{w}{\rho \times t} \frac{[2a + 2c]}{[2(a \times b) + 2(b \times c) + 2(a \times c)]^2} \quad (6-30)$$

$$\frac{\partial y}{\partial c} = \frac{w}{\rho \times t} \frac{[2a + 2b]}{[2(a \times b) + 2(b \times c) + 2(a \times c)]^2} \quad (6-31)$$

The maximum error in the corrosion rate is estimated by calculating numeric values of the partial derivatives from expected values of the independent variables, multiplication of each partial derivative by the corresponding error in independent variable (Δw , $\Delta \rho$, Δt , Δa , Δb and Δc), and summation of the resulting products. Note that there is some uncertainty in the density, which is accounted for. The error based upon this method is shown in Tables 11 through 15. From the estimated errors given in Table 11, it is concluded that the typical uncertainty observed in weight loss and dimensional measurements prevent determination of corrosion rates less than 46 nanometers per year (crevice sample worst case). This estimate of error is believed to correspond to about one standard deviation (1σ). Therefore, any measured corrosion rate less than 184 nanometers per year (4σ) will not be distinguishable from measurement error.

GC rates determined from measurements of weight loss in the LTCTF are shown in Figures 19 and 20. The LTCTF and results from that facility are described in detail in previous publications by the YMP (Estill 1998). The maximum rates shown in Figure 20 appear to be less than about 350 nanometers per year, slightly greater than the estimated 4σ value. Any rate less than 350 nm per year guarantees that the DS (wall thickness of 2 cm) will not fail by GC. Note that the impact of the hole in the crevice samples on the error analysis was believed to be relatively small and, therefore, neglected.

Table 11. Summary of Error Analysis for Corrosion Rates Based Upon Weight Loss Measurements

| | Assumed Wt. Loss | | 0.0001 g | 0.0010 g | 0.0100 g |
|------|----------------------|---------------|---------------------|---------------------|---------------------|
| | | | Δy | Δy | Δy |
| Case | Sample Configuration | Exposure Time | nm yr ⁻¹ | nm yr ⁻¹ | nm yr ⁻¹ |
| 1 | Crevice | 6 month | 23.64 | 25.72 | 46.47 |
| 2 | Weight Loss | 6 month | 44.89 | 48.94 | 89.41 |
| 3 | Crevice | 12 month | 11.58 | 12.50 | 21.70 |
| 4 | Weight Loss | 12 month | 22.00 | 23.79 | 41.78 |

Table 12. Error Analysis for LTCTF Corrosion Rates–Definitions

| Parameter | Parameter Definition | Units |
|---|--|--|
| w | Weight loss | g |
| ρ | Density | g cm^{-3} |
| t | Exposure time | hr |
| a | Length | in |
| b | Width | in |
| c | Thickness | in |
| a | Length | cm |
| b | Width | cm |
| c | Thickness | cm |
| | | |
| $\partial y/\partial w$ | Partial derivative or rate with respect to weight loss | $\text{cm g}^{-1} \text{hr}^{-1}$ |
| $\partial y/\partial \rho$ | Partial derivative of rate with respect to density | $\text{cm}^4 \text{g}^{-1} \text{hr}^{-1}$ |
| $\partial y/\partial t$ | Partial derivative of rate with respect to exposure time | cm hr^{-2} |
| $\partial y/\partial a$ | Partial derivative of rate with respect to length | hr^{-1} |
| $\partial y/\partial b$ | Partial derivative of rate with respect to width | hr^{-1} |
| $\partial y/\partial c$ | Partial derivative of rate with respect to thickness | hr^{-1} |
| Δw | Error in weight loss | g |
| $\Delta \rho$ | Error in density | g cm^{-3} |
| Δt | Error in exposure time | hr |
| Δa | Error in length | cm |
| Δb | Error in width | cm |
| Δc | Error in thickness | cm |
| $(\partial y/\partial w) \times (\Delta w)$ | Weight loss product | cm |
| $(\partial y/\partial \rho) \times (\Delta \rho)$ | Density product | cm |
| $(\partial y/\partial t) \times (\Delta t)$ | Exposure time product | cm |
| $(\partial y/\partial a) \times (\Delta a)$ | Length product | cm |
| $(\partial y/\partial b) \times (\Delta b)$ | Width product | cm |
| $(\partial y/\partial c) \times (\Delta c)$ | Thickness product | cm |
| | | |
| Δy | Sum of all products | cm hr^{-1} |
| Δy | Sum of all products | $\mu\text{m yr}^{-1}$ |
| Δy | Sum of all products | nm yr^{-1} |

Table 13. Error Analysis for LTCTF Corrosion Rates—Assume Weight Loss of 0.0001 Grams

| Parameter | Crevice 6 mo. | Wt. Loss 6 mo. | Crevice 12 mo. | Wt. Loss 12 mo. |
|---|---------------|----------------|----------------|-----------------|
| w | 0.0001 | 0.0001 | 0.0001 | 0.0001 |
| ρ | 4.52 | 4.52 | 4.52 | 4.52 |
| t | 4296 | 4296 | 8760 | 8760 |
| a | 2.0000 | 2.0000 | 2.0000 | 2.0000 |
| b | 2.0000 | 1.0000 | 2.0000 | 1.0000 |
| c | 0.1200 | 0.1200 | 0.1200 | 0.1200 |
| a | 5.0800 | 5.0800 | 5.0800 | 5.0800 |
| b | 5.0800 | 2.5400 | 5.0800 | 2.5400 |
| c | 0.3048 | 0.3048 | 0.3048 | 0.3048 |
| | | | | |
| $\partial y/\partial w$ | 8.9089E-07 | 1.6912E-06 | 4.3690E-07 | 8.2937E-07 |
| $\partial y/\partial \rho$ | 1.9710E-11 | 3.7415E-11 | 9.6659E-12 | 1.8349E-11 |
| $\partial y/\partial t$ | 2.0738E-14 | 3.9366E-14 | 4.9874E-15 | 9.4677E-15 |
| $\partial y/\partial a$ | 1.6598E-11 | 3.1598E-11 | 8.1397E-12 | 1.5496E-11 |
| $\partial y/\partial b$ | 1.6598E-11 | 5.9811E-11 | 8.1397E-12 | 2.9332E-11 |
| $\partial y/\partial c$ | 3.1316E-11 | 8.4638E-11 | 1.5358E-11 | 4.1507E-11 |
| | | | | |
| Δw | 0.0003 | 0.0003 | 0.0003 | 0.0003 |
| $\Delta \rho$ | 0.1 | 0.1 | 0.1 | 0.1 |
| Δt | 24 | 24 | 24 | 24 |
| Δa | 0.00254 | 0.00254 | 0.00254 | 0.00254 |
| Δb | 0.00254 | 0.00254 | 0.00254 | 0.00254 |
| Δc | 0.00254 | 0.00254 | 0.00254 | 0.00254 |
| | | | | |
| $(\partial y/\partial w) \times (\Delta w)$ | 2.6727E-10 | 5.0735E-10 | 1.3107E-10 | 2.4881E-10 |
| $(\partial y/\partial \rho) \times (\Delta \rho)$ | 1.9710E-12 | 3.7415E-12 | 9.6659E-13 | 1.8349E-12 |
| $(\partial y/\partial t) \times (\Delta t)$ | 4.9770E-13 | 9.4479E-13 | 1.1970E-13 | 2.2722E-13 |
| $(\partial y/\partial a) \times (\Delta a)$ | 4.2158E-14 | 8.0259E-14 | 2.0675E-14 | 3.9360E-14 |
| $(\partial y/\partial b) \times (\Delta b)$ | 4.2158E-14 | 1.5192E-13 | 2.0675E-14 | 7.4503E-14 |
| $(\partial y/\partial c) \times (\Delta c)$ | 7.9543E-14 | 2.1498E-13 | 3.9009E-14 | 1.0543E-13 |
| | | | | |
| Δy | 2.6990E-10 | 5.1249E-10 | 1.3224E-10 | 2.5109E-10 |
| Δy | 2.3643E-02 | 4.4894E-02 | 1.1584E-02 | 2.1996E-02 |
| Δy | 2.3643E+01 | 4.4894E+01 | 1.1584E+01 | 2.1996E+01 |

Table 14. Error Analysis for LTCTF Corrosion Rates—Assume Weight Loss of 0.001 Grams

| Parameter | Crevice 6 mo. | Wt. Loss 6 mo. | Crevice 12 mo. | Wt. Loss 12 mo. |
|---|---------------|----------------|----------------|-----------------|
| w | 0.0010 | 0.0010 | 0.0010 | 0.0010 |
| ρ | 4.52 | 4.52 | 4.52 | 4.52 |
| t | 4296 | 4296 | 8760 | 8760 |
| a | 2.0000 | 2.0000 | 2.0000 | 2.0000 |
| b | 2.0000 | 1.0000 | 2.0000 | 1.0000 |
| c | 0.1200 | 0.1200 | 0.1200 | 0.1200 |
| a | 5.0800 | 5.0800 | 5.0800 | 5.0800 |
| b | 5.0800 | 2.5400 | 5.0800 | 2.5400 |
| c | 0.3048 | 0.3048 | 0.3048 | 0.3048 |
| $\partial y/\partial w$ | 8.9089E-07 | 1.6912E-06 | 4.3690E-07 | 8.2937E-07 |
| $\partial y/\partial \rho$ | 1.9710E-10 | 3.7415E-10 | 9.6659E-11 | 1.8349E-10 |
| $\partial y/\partial t$ | 2.0738E-13 | 3.9366E-13 | 4.9874E-14 | 9.4677E-14 |
| $\partial y/\partial a$ | 1.6598E-10 | 3.1598E-10 | 8.1397E-11 | 1.5496E-10 |
| $\partial y/\partial b$ | 1.6598E-10 | 5.9811E-10 | 8.1397E-11 | 2.9332E-10 |
| $\partial y/\partial c$ | 3.1316E-10 | 8.4638E-10 | 1.5358E-10 | 4.1507E-10 |
| Δw | 0.0003 | 0.0003 | 0.0003 | 0.0003 |
| $\Delta \rho$ | 0.1 | 0.1 | 0.1 | 0.1 |
| Δt | 24 | 24 | 24 | 24 |
| Δa | 0.00254 | 0.00254 | 0.00254 | 0.00254 |
| Δb | 0.00254 | 0.00254 | 0.00254 | 0.00254 |
| Δc | 0.00254 | 0.00254 | 0.00254 | 0.00254 |
| $(\partial y/\partial w) \times (\Delta w)$ | 2.6727E-10 | 5.0735E-10 | 1.3107E-10 | 2.4881E-10 |
| $(\partial y/\partial \rho) \times (\Delta \rho)$ | 1.9710E-11 | 3.7415E-11 | 9.6659E-12 | 1.8349E-11 |
| $(\partial y/\partial t) \times (\Delta t)$ | 4.9770E-12 | 9.4479E-12 | 1.1970E-12 | 2.2722E-12 |
| $(\partial y/\partial a) \times (\Delta a)$ | 4.2158E-13 | 8.0259E-13 | 2.0675E-13 | 3.9360E-13 |
| $(\partial y/\partial b) \times (\Delta b)$ | 4.2158E-13 | 1.5192E-12 | 2.0675E-13 | 7.4503E-13 |
| $(\partial y/\partial c) \times (\Delta c)$ | 7.9543E-13 | 2.1498E-12 | 3.9009E-13 | 1.0543E-12 |
| Δy | 2.9359E-10 | 5.5869E-10 | 1.4274E-10 | 2.7162E-10 |
| Δy | 2.5719E-02 | 4.8941E-02 | 1.2504E-02 | 2.3794E-02 |
| Δy | 2.5719E+01 | 4.8941E+01 | 1.2504E+01 | 2.3794E+01 |

Table 15. Error Analysis for LTCTF Corrosion Rates—Assume Weight Loss of 0.01 Grams

| Parameter | Crevice 6 mo. | Wt. Loss 6 mo. | Crevice 12 mo. | Wt. Loss 12 mo. |
|---|---------------|----------------|----------------|-----------------|
| w | 0.0100 | 0.0100 | 0.0100 | 0.0100 |
| ρ | 4.52 | 4.52 | 4.52 | 4.52 |
| t | 4296 | 4296 | 8760 | 8760 |
| a | 2.0000 | 2.0000 | 2.0000 | 2.0000 |
| b | 2.0000 | 1.0000 | 2.0000 | 1.0000 |
| c | 0.1200 | 0.1200 | 0.1200 | 0.1200 |
| a | 5.0800 | 5.0800 | 5.0800 | 5.0800 |
| b | 5.0800 | 2.5400 | 5.0800 | 2.5400 |
| c | 0.3048 | 0.3048 | 0.3048 | 0.3048 |
| | | | | |
| $\partial y/\partial w$ | 8.9089E-07 | 1.6912E-06 | 4.3690E-07 | 8.2937E-07 |
| $\partial y/\partial \rho$ | 1.9710E-09 | 3.7415E-09 | 9.6659E-10 | 1.8349E-09 |
| $\partial y/\partial t$ | 2.0738E-12 | 3.9366E-12 | 4.9874E-13 | 9.4677E-13 |
| $\partial y/\partial a$ | 1.6598E-09 | 3.1598E-09 | 8.1397E-10 | 1.5496E-09 |
| $\partial y/\partial b$ | 1.6598E-09 | 5.9811E-09 | 8.1397E-10 | 2.9332E-09 |
| $\partial y/\partial c$ | 3.1316E-09 | 8.4638E-09 | 1.5358E-09 | 4.1507E-09 |
| | | | | |
| Δw | 0.0003 | 0.0003 | 0.0003 | 0.0003 |
| $\Delta \rho$ | 0.1 | 0.1 | 0.1 | 0.1 |
| Δt | 24 | 24 | 24 | 24 |
| Δa | 0.00254 | 0.00254 | 0.00254 | 0.00254 |
| Δb | 0.00254 | 0.00254 | 0.00254 | 0.00254 |
| Δc | 0.00254 | 0.00254 | 0.00254 | 0.00254 |
| | | | | |
| $(\partial y/\partial w) \times (\Delta w)$ | 2.6727E-10 | 5.0735E-10 | 1.3107E-10 | 2.4881E-10 |
| $(\partial y/\partial \rho) \times (\Delta \rho)$ | 1.9710E-10 | 3.7415E-10 | 9.6659E-11 | 1.8349E-10 |
| $(\partial y/\partial t) \times (\Delta t)$ | 4.9770E-11 | 9.4479E-11 | 1.1970E-11 | 2.2722E-11 |
| $(\partial y/\partial a) \times (\Delta a)$ | 4.2158E-12 | 8.0259E-12 | 2.0675E-12 | 3.9360E-12 |
| $(\partial y/\partial b) \times (\Delta b)$ | 4.2158E-12 | 1.5192E-11 | 2.0675E-12 | 7.4503E-12 |
| $(\partial y/\partial c) \times (\Delta c)$ | 7.9543E-12 | 2.1498E-11 | 3.9009E-12 | 1.0543E-11 |
| | | | | |
| Δy | 5.3052E-10 | 1.0207E-09 | 2.4773E-10 | 4.7695E-10 |
| Δy | 4.6474E-02 | 8.9413E-02 | 2.1702E-02 | 4.1781E-02 |
| Δy | 4.6474E+01 | 8.9413E+01 | 2.1702E+01 | 4.1781E+01 |
| | | | | |

6.5.4 Composite Representation of General Corrosion (GC) Rates for Drip Shield

A simple and defensible representation of the observed GC rates is recommended. The distribution of GC rates determined from “Weight Loss Samples” (Figure 19) and the distribution of GC rates determined from “Crevice Samples” (Figure 20) are combined into a single distribution. All negative rates are eliminated, and the entire distribution is assumed to be due to uncertainty. From Figure 21, it can be seen that the rate at the 50th percentile is approximately 25 nanometers per year, the rate at the 90th percentile is approximately 100 nanometers per year, and the maximum rate is less than 350 nanometers per year. About 10% of the values fall between 100 and 350 nanometers per year. Figure 21 shows that the logarithm of the observed GC rates obeys a rectangular distribution.

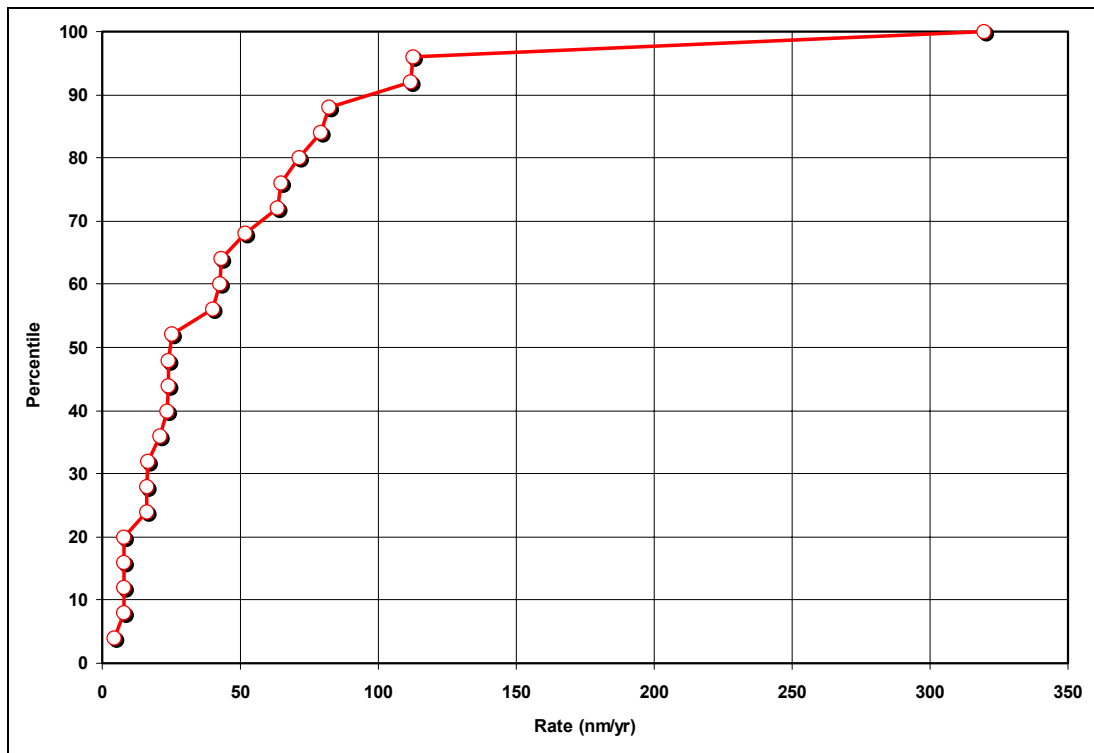


Figure 21. Distribution of General Corrosion Rates of Ti Grade 16: LTCTF 12-Month Weight Loss and Crevice Samples—No Negative Rates

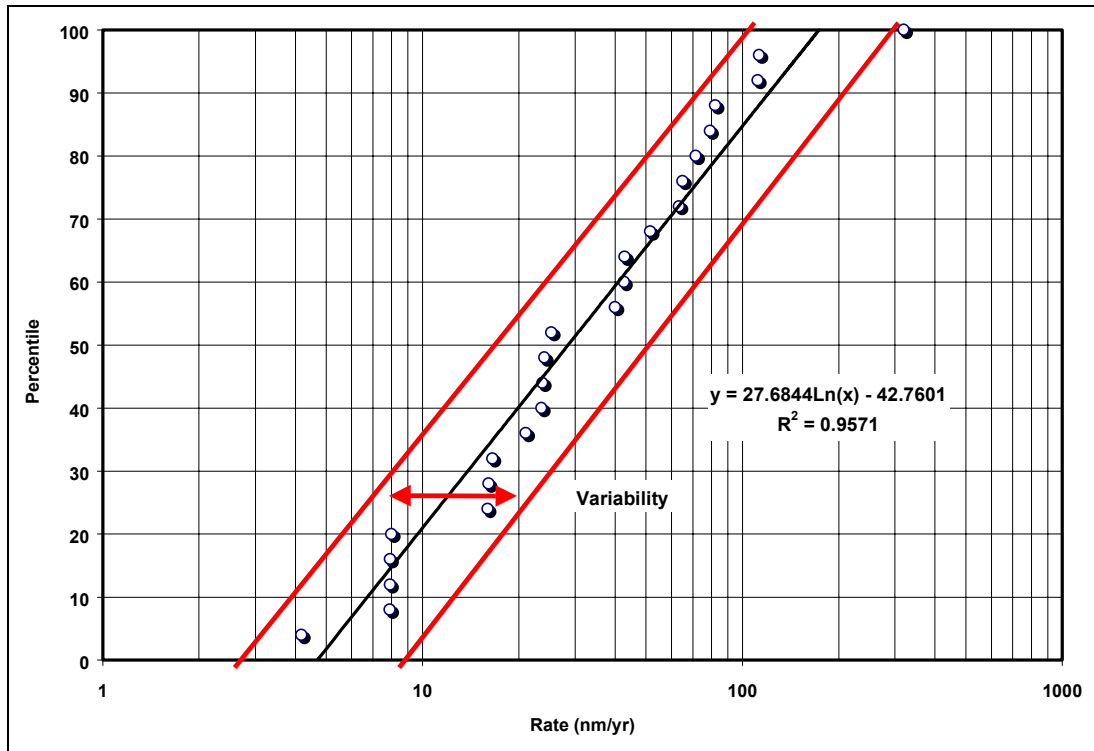


Figure 22. Distribution of Logarithm of General Corrosion Rates of Ti Grade 16: LTCTF 12-Month Weight Loss and Crevice Samples—No Negative Rates

The distribution function y is given in percent and is described by the following correlation:

$$y = 27.6844 \ln(x) - 42.7601 \quad R^2 = 0.9571 \quad (\text{Eq. 34})$$

where x is the GC rate in nanometers per year. This distribution function is truncated above 100% to avoid nonsensical values. It is assumed that the variability obeys a triangular distribution function:

$$F(x) = \frac{(x-a)^2}{(b-a)(c-a)} \quad a \leq x \leq c \quad (\text{Eq. 35})$$

or

$$F(x) = 1 - \frac{(b-x)^2}{(b-a)(b-c)} \quad c \leq x \leq b \quad (\text{Eq. 36})$$

where the mode is the parameter c . The probability density function is then:

$$f(x) = \frac{2(x-a)}{(b-a)(c-a)} \quad a \leq x \leq c \quad (\text{Eq. 37})$$

or

$$f(x) = \frac{2(b-x)}{(b-a)(b-c)} \quad c \leq x \leq b \quad (\text{Eq. 38})$$

The mean and variance are:

$$\mu = \frac{(a+b+c)}{3} \quad (\text{Eq. 39})$$

and

$$\sigma^2 = \frac{a^2 + b^2 + c^2 - ab - ac - bc}{18} \quad (\text{Eq. 40})$$

The mode, c , is identical the GC rate, x , defined in the discussion of $U(x)$. The values of the parameters a and b are determined from the two lines bounding the correlation for $U(x)$.

6.6 DISSOLVED OXYGEN IN THE LONG TERM CORROSION TEST FACILITY

In principle, the corrosion rates observed in the LTCTF should depend upon the concentration of dissolved oxygen. The anodic dissolution of a metal requires a corresponding amount of cathodic reduction. Typically, dissolved oxygen or hydrogen ion is reduced. However, as previously discussed, other reactants such as hydrogen peroxide (due to gamma radiolysis) can also be reduced. Figure 30 in the companion AMR on GC and LC of the WPOB (CRWMS M&O 2000c) shows a comparison of dissolved oxygen measurements in the LTCTF to published data for synthetic geothermal brine (Cramer 1974). The published data spans the range of temperature from 20 to 300°C and spans the range of oxygen partial pressures from 1 to 30 psi. Note that the partial pressure of oxygen in the atmosphere is about 3 psi. The points representing measurements from the LTCTF tanks are superimposed upon the published data. Clearly, the SDW, SCW, and SAW appear to be saturated (4 to 10 ppm dissolved oxygen).

6.7 CREVICE CORROSION

The hydrolysis of dissolved metal in crevices can lead to the accumulation of H^+ and the corresponding suppression of pH. For example, $pH < 2$ has been observed in crevices made of stainless steel, as discussed by Sedriks (1996). In the case of titanium-based alloys, such low pH can exacerbate any problems due to HIC (Ikeda et al. 1994; Shoesmith et al. 1995). Titanium and its alloys are usually passive over a very broad range of pH and electrochemical potential, as illustrated by Pourbaix (1974). However, passivity can be lost under extreme general or local conditions. For example, the potential-pH diagram that accounts for the formation of both hydrated TiO_2 and $Ti(OH)_3$ show a region of active dissolution over a broad range of electrochemical potentials at low pH. The theoretical domains of corrosion, immunity, and passivation at 25°C show regions of active dissolution below pH 2. Within the thermodynamic

limits of water, titanium is expected to dissolve as either Ti^{3+} or TiO^{2+} . Oxyanions such as $HTiO_3^-$, TiO_4^{2-} , and $HTiO_4^-$ may form, but require very alkaline conditions.

This present work is directed at high-level waste packages made of titanium-based materials. Insight into the localized corrosion and hydrogen-induced cracking of relevant titanium-based alloys (especially Ti Grade 2) is obtainable from publications of Shoemith et al. (1995) and Ikeda et al. (1994).

In regard to the conclusions of Shoemith et al. (1995) and Ikeda et al. (1994), it is important to note that the depletion of oxygen is anticipated in the Canadian repository (sealed in compacted clay and sand). In sharp contrast, we anticipate the availability of oxygen at Yucca Mountain over the entire waste package life. Following the logic outlined by the Canadian high-level waste program, the inner titanium barrier could be threatened by crevice corrosion and HIC after the outer barrier is breached. It is noteworthy that in cases where a titanium-based alloy (Ti Grade 12) has been galvanically coupled to carbon steel (A516) in acidic brine (5 wt.% NaCl, pH 2.7, 30-80°C), very cathodic potentials were achieved (-0.785 V vs. Ag/AgCl) (Roy et al. 1997). Relatively high cathodic currents were achieved on the titanium surface, ranging from 17 to 56 $\mu A\ cm^{-2}$. The partitioning of this current between oxygen reduction, hydrogen evolution, and hydrogen absorption is unknown. It should also be noted that the presence of any recombination poison, which might be present in complicated ground waters, could dramatically increase hydrogen charging rates. While experimental determinations of the crevice pH have been made in the case of stainless steels, work for titanium-based alloys must still be done.

If the threshold potential for localized attack is exceeded, a corrosion rate representative of LC must be assumed. Unfortunately, due to the outstanding corrosion resistance of Ti Grade 7, relatively little data exists for such LC under plausible conditions. From the reviewed literature (Gdowski 1997, Table 15.1), a crevice corrosion depth of 250 microns was observed in a crevice formed from Ti-0.2%Pd and PTFE after a 582 day exposure in deaerated brine at 90°C (157 microns per year). In a metal-metal crevice, a crevice corrosion depth of 70 microns was observed in a crevice formed from Ti-0.2%Pd after 489 days (52 microns per year). Other more severe values are also given by Gdowski (1997, Appendix A) and are shown in Table 16 below. This table represents the range of corrosion rates observed in acidic environments, such as those anticipated in crevices. It is expected that a rectangular distribution based on this table is applicable for the LC of Ti Grade 7.

Table 16. Assumed Distribution of Localized Corrosion Rates for Ti Grade 7

| Percentile | Localized Corrosion Rate (microns per year) | Conditions |
|-------------------|---|---|
| 0 th | 490 | 19% HCl + 4% FeCl ₃ + 4% MgCl ₂ at 82°C |
| 100 th | 1120 | Boiling 3:1 Aqua Regia |

DTN: LL981212005924.062 (Non-Q)

6.8 GAMMA RADIOLYSIS

As discussed in the companion AMR on GC and LC of the WPOB, ambient-temperature CP studies have been performed with 316L samples in 0.018 M NaCl solution during exposure to

3.5 Mrad hr⁻¹ gamma radiation (Glass et al. 1986). This investigator found that the corrosion current shifted in the anodic direction by approximately 200 mV, with very little increase in the corresponding corrosion current density. However, the separation between the corrosion potential and the threshold for localized attack decreased slightly. This shift in corrosion potential was shown to be due to the formation of hydrogen peroxide and was subsequently confirmed by others (Kim 1999). In this case, ambient-temperature CP of 316 stainless steel in acidic (pH~2) 1.5 M NaCl during exposure to 0.15 Mrad hr⁻¹ gamma radiation showed a 100 mV anodic shift in the corrosion potential, with very little effect on the corrosion current. While the E_{corr} shift for Ti Grade 7 will probably be somewhat different than that of 316L, it is doubtful that the shift will ever be sufficient for E_{corr} to exceed $E_{critical}$. Thus, even in the presence of gamma radiolysis, only GC would be expected. No significant effect of gamma radiolysis on GC rates of titanium-based alloys is expected.

6.9 MICROBIALLY INFLUENCED CORROSION

It has been observed that titanium-based alloys are very resistant to MIC. Furthermore, it is believed that microbial growth in the repository will be limited by the availability of nutrients. The assertion regarding the resistance of titanium to MIC is well supported by the published literature. According to Shoosmith et al. (1995), the initiation of crevice corrosion under biofilms has never been observed for titanium. However, since titanium is not biotoxic such a process is not ruled out. If it is found that MIC does occur, it will be accounted for by its localized effects on pH, E_{corr} , $E_{critical}$, and penetration rate. The effect of MIC on penetration rate will be accounted for through the factor G_{MIC} , as discussed in the companion AMR on GC and LC of the WPOB. The possible acceleration of abiotic corrosion processes by microbial growth has also been a concern. Bacteria and fungi alter local environment in biofilm. For example, H⁺ is known to be generated by bacterial isolates from Yucca Mountain. Any lowering of pH could tend to exacerbate HIC. Furthermore, thiobacillus ferrooxidans oxidize Fe²⁺, while geobacter metallireducens reduce Fe³⁺. Other microbes can reduce SO₄²⁻ and produce S²⁻ (Horn et al. 1998). In the future, we hope to calculate concentration transients in biofilms with a relatively simple bioreactor model. It is not believed that these effects will substantially impact the resistance of this material.

6.10 MODEL VALIDATION

Model validation is accomplished in part by comparing experimental measurements of key model parameters to corroborative data that has been published in the open scientific literature. For example, GC rates, corrosion potentials, threshold potentials, and assumed crevice pH values are compared to those published for both Ti Grade 7 and similar alloys in somewhat similar environments (NaCl solutions, sea water, etc.). Validation of the overall model will require extensive review of calculations performed with the model based upon this process-level model. That model will be addressed in a companion AMR. Calculated corrosion rates will be compared to experimental measurements to make sure that those rates are reasonable. Absolute validation of a model intended for the prediction of a service life of 10,000 years may not be possible. These models are based upon the best knowledge and insight into the materials and systems available at the present time. As our state of understanding improves, predictions will inevitably be updated to reflect such advancement. Through the implementation of probabilistic

calculations that embody the integrated corrosion models provided here, an attempt is made to compensate for uncertainty in the data.

6.11 SUMMARY OF MODEL

The model for the GC and LC of Ti Grade 7 is summarized in Figure 1. The threshold RH is first used to determine whether or not DOX will take place. If DOX is determined to occur, the logarithmic growth law represented by Equations 13 through 22 is then used to calculate the corrosion rate as a function of temperature. If the threshold RH is exceeded, HAC will occur in the absence of dripping water, and APC will occur in the presence of dripping water. If APC is assumed to occur, the corrosion and critical potentials are used to determine whether the mode of attack is general or localized. The correlation of data represented by Equation 26 and Table 5 are used as the basis for estimating these potentials at the 50th percentile. Since the material specifications will be based partly on the measured corrosion and critical potentials, it will be assumed that these potentials will be uniformly distributed about the 50th percentile values determined from the correlation. For example, the 0th and 100th percentile values of E_{corr} will be assumed to be at E_{corr} (50th percentile) \pm 500 mV. This acceptable margin was determined by splitting the differences for SDW shown in Table 6. Similarly, the 0th and 100th percentile values of $E_{critical}$ will be assumed to be at $E_{critical}$ (50th percentile) \pm 500 mV. Material falling outside of these specified ranges will not be accepted. If the comparison of E_{corr} to $E_{critical}$ indicates GC, the distribution of rates determined from the LTCTF will be used as the basis of the GC rate.

7. CONCLUSIONS

Ti Grade 7 is an exceptional CRM, with a very stable passive film. Based upon exposures in the LTCTF, it has been concluded that the GC and oxidation rates of Ti Grade 7 are essentially below the level of detection. In any event, over the 10,000-year life of the repository, GC and oxidation should not be life limiting. The large separation between measured corrosion and threshold potentials indicate that localized breakdown of the passive film is unlikely under plausible conditions, even in SSW at 120°C.

With exposures of two years, no significant evidence of crevice corrosion has been observed with Ti Grade 16 in SDW, SCW, and SAW at temperatures up to 90°C, though many of the samples have a beautiful green patina. A model has been presented, with parameters determined experimentally, that should enable performance assessment to account for the GC and LC of this material. A feature of this model is the use of the materials specification to limit the range of corrosion and threshold potentials, thereby making sure that substandard materials prone to localized attack are avoided. Uncertainties associated with the model based on the electrochemical measurements and the weight loss measurements are addressed in Sections 6.5.1 and 6.5.3, respectively.

The data tracking numbers (DTNs) of the associated developed data and description are listed below:

DTN: LL000209205924.128. Summary Corrosion Study Parameters for Titanium grade 7 (Ti Gr 7).

DTN: LL000209305924.129. Summary Corrosion Study Parameters of LTCF for Ti Gr 16.

This data supercedes data previously identified in DTN: LL990805605924.087.

This document may be affected by technical product input information that requires confirmation. Any changes to the document that may occur as a result of completing the confirmation activities will be reflected in subsequent revisions. The status of the input information quality may be confirmed by review of the Document Input Reference System database.

8. INPUTS AND REFERENCES

8.1 DOCUMENTS CITED

Bard, A.J. and Faulkner, L.R. 1980. "Liquid Junction Potentials." Section 2.3 of *Electrochemical Methods, Fundamentals and Applications*. New York, New York: John Wiley & Sons. TIC: 245183.

Cramer, S.D. 1974. "The Solubility of Oxygen in Geothermal Brines." *Corrosion Problems in Energy Conversion and Generation*. Tedmen, C.S., Jr., ed. 251-262. Princeton, New Jersey: Electrochemical Society. TIC: 245180.

CRWMS M&O 1999a. *Monitored Geologic Repository Project Description Document*. B00000000-01717-1705-00003 REV 00 DCN 01. Las Vegas, Nevada: CRWMS M&O. ACC: MOL.19991117.0160.

CRWMS M&O 1999b. *General Corrosion and Localized Corrosion of the Drip Shield*. Work Direction and Planning Document. Las Vegas, Nevada: CRWMS M&O. ACC: MOL.19990708.0231.

CRWMS M&O 1999c. *Classification of the MGR Ex-Container System*. ANL-XCS-SE-000001 REV 00. Las Vegas, Nevada: CRWMS M&O. ACC: MOL.19990928.0221.

CRWMS M&O 1999d. *1101213PM7 Waste Package Analyses & Models - PMR*. Activity Evaluation, September 21, 1999. Las Vegas, Nevada: CRWMS M&O. ACC: MOL.19991012.0219.

CRWMS M&O 1999e. *Waste Package Materials Properties*. BBA000000-01717-0210-00017 REV 00. Las Vegas, Nevada: CRWMS M&O. ACC: MOL.19990407.0172.

CRWMS M&O 2000a. *Environment on the Surfaces of the Drip Shield and Waste Package Outer Barrier*. Input Transmittal WP-LNL-00018.T. Las Vegas, Nevada: CRWMS M&O. ACC: MOL.20000118.0316.

CRWMS M&O 2000b. *Aging and Phase Stability of Waste Package Outer Barrier Model*. Input Transmittal WP-LNL-00019.T. Las Vegas, Nevada: CRWMS M&O. ACC: MOL.20000118.0317.

CRWMS M&O 2000c. *General Corrosion and Localized Corrosion of Waste Package Outer Barrier*. ANL-EBS-MD-000003 REV 00. Las Vegas, Nevada: CRWMS M&O. ACC: MOL.20000202.0172.

CRWMS M&O 2000d. *Emplacement Drift System Description Document*. SDD-EDS-SE-000001 REV 00. Las Vegas, Nevada: CRWMS M&O. ACC: MOL.20000121.0119.

DOE (U.S. Department of Energy) 2000. *Quality Assurance Requirements and Description*. DOE/RW-0333P, Rev. 9. Washington, D.C.: U.S. Department of Energy, Office of Civilian Radioactive Waste Management. ACC: MOL.19991028.0012.

Estill, J.C. 1998. "Long-Term Corrosion Studies ." 2.2 of *Engineered Materials Characterization Report*. McCright, R.D., ed. UCRL-ID-119564 Volume 3 Rev.1.1. Livermore, California: Lawrence Livermore National Laboratory. ACC: MOL.19981222.0137.

Gartland, P.O. 1997. "A Simple Model of Crevice Corrosion Propagation for Stainless Steels in Seawater." *Corrosion* 97. 417/1 to 417/17. Houston, Texas: NACE International. TIC: 245216.

Gdowski, G.E. 1997. *Degradation Mode Survey Candidate Titanium - Base Alloys for Yucca Mountain Project Waste Package Materials*. UCRL-ID-121191, Rev. 1. Livermore, California: Lawrence Livermore National Laboratory. ACC: MOL.19980120.0053.

Glass, R.S.; Overturf, G.E.; Van Konynenburg, R.A.; and McCright, R.D. 1986. "Gamma Radiation Effects on Corrosion-I. Electrochemical Mechanisms for the Aqueous Corrosion Processes of Austenitic Stainless Steels Relevant to Nuclear Waste Disposal in Tuff." *Corrosion Science*, 26, (8), 577-590. Oxford, Great Britain: Pergamon. TIC: 226179.

Gruss, K.A.; Cragolino, G.A.; Dunn, D.S.; and Sridhar, N. 1998. "Repassivation Potential for Localized Corrosion of Alloys 625 and C22 in Simulated Repository Environments." *Proceedings of Corrosion 98, March 22-27, 1998, San Diego, California*. 149/1 to 149/15. Houston, Texas: NACE International. TIC: 237149.

Harrar, J.E.; Carley, J.F.; Isherwood, W.F.; and Raber, E. 1990. *Report of the Committee to Review the Use of J-13 Well Water in Nevada Nuclear Waste Storage Investigations*. UCID-21867. Livermore, California: Lawrence Livermore National Laboratory. ACC: NNA.19910131.0274.

Horn, J.M.; Rivera, A.; Lian, T.; and Jones, D. 1998. "MIC Evaluation and Testing for the Yucca Mountain Repository." *Proceedings of Corrosion 98, National Association of Corrosion Engineers, March 22-27, San Diego, California*. 152/2 to 152/14. Houston, Texas: NACE International. TIC: 237146.

Ikeda, B.M.; Bailey, M.G.; Quinn, M.J.; and Shoesmith, D.W. 1994. "The Development of an Experimental Data Base for the Lifetime Predictions of Titanium Nuclear Waste Containers." *Application of Accelerated Corrosion Tests to Service Life Prediction of Materials*. Cragolino, G. and Sridhar, N., eds. ASTM STP 1194. Pages 126-142. Philadelphia, Pennsylvania: American Society for Testing and Materials. Library Tracking Number-L1389.

- Jones, D.A. 1996. *Principles and Prevention of Corrosion*. 2nd Edition. Upper Saddle River, New Jersey: Prentice Hall. TIC: 241233.
- Kim, Y-J. 1999. "In-Situ Electrochemical Impedance Measurement of Oxide Film on 304 SS in 288°C Water." *Corrosion 99. Paper No. 437*, 1-11. Houston, Texas: NACE International. TIC: 246024.
- Landolt, D. 1995. "Introduction to Surface Reactions: Electrochemical Basis of Corrosion." Chapter 1 of *Corrosion Mechanisms in Theory and Practice*. Marcus, P. and Oudar, J., eds. New York, New York: Marcel Dekker. TIC: 104415.
- Leygraf, C. 1995. "Atmospheric Corrosion." Chapter 12 of *Corrosion Mechanisms in Theory and Practice*. Marcus, P. and Oudar, J., eds. New York, New York: Marcel Dekker. TIC: 104415.
- Pohlman, S.L. 1987. *Atmospheric Corrosion*. Volume 13 of *Metals Handbook*. 9th Edition. Pages 80-103. Metals Park, Ohio: ASM International. TIC: 209807.
- Pourbaix, M. 1974. *Atlas of Electrochemical Equilibria in Aqueous Solutions*. Houston, Texas: National Association of Corrosion Engineers. TIC: 208955.
- Roy, A. K.; Fleming, D.L.; and Lum, B.Y. 1997. *Galvanic Corrosion Study of Container Materials Using Zero Resistance Ammeter*. UCRL-JC-128475. Livermore, California: Lawrence Livermore National Laboratory. ACC: MOL.19980121.0137.
- Scully, J.R.; Hudson, J.L.; Lunt, T.; Ilevbare, G.; and Kehler, B. 1999. *Localized Corrosion Initiation and Transition to Stabilization in Alloys 625 and C-22*. Charlottesville, Virginia: University of Virginia. TIC: 246630.
- Sedriks, A.J. 1996. *Corrosion of Stainless Steels*. 2nd Edition. 179, 377. New York, New York: John Wiley & Sons. TIC: 245121.
- Shoesmith, D.W.; Ikeda, B.M.; Bailey, M.G.; Quinn, M.J.; and LeNeveu, D.M. 1995. *A Model for Predicting the Lifetimes of Grade-2 Titanium Nuclear Waste Containers*. AECL-10973. Pinawa, Manitoba, Canada: Atomic Energy of Canada Limited. TIC: 226419.
- Walton, J.C.; Cragolino, G.; and Kalandros, S.K. 1996. "A Numerical Model of Crevice Corrosion for Passive and Active Metals." *Corrosion Science*, 38, (1), 1-18. Amsterdam, The Netherlands: Pergamon. TIC: 233439.

Weast, R.C. and Astle, M.J., eds. 1978. *CRC Handbook of Chemistry and Physics*. 59th Edition. pp. D-265, D-299, D-300, -304 , F-61 and F-62. Boca Raton, Florida: CRC Press. TIC: 246395.

Welsch, G.; Smialek, J.L.; Doychak, J.; Waldman, J.; and Jacobson, N.S. 1996. "High Temperature Oxidation and Properties." Chapter 2 of *Oxidation and Corrosion of Intermetallic Alloys*. Welsch, G. and Desai, P.D.: eds. West Lafayette, Indiana: Purdue University. TIC: 245280.

8.2 CODES, STANDARDS, REGULATIONS, AND PROCEDURES

AP-3.10Q, Rev. 02, ICN 0. *Analyses and Models*. Washington D.C., Washington D.C.: Office of Civilian Radioactive Waste Management. ACC: MOL.20000217.0246.

AP-SI.1Q, Rev. 2, ICN 4. *Software Management*. Washington, D.C.: U.S. Department of Energy, Office of Civilian Radioactive Waste Management. ACC: MOL.20000223.0508.

ASTM G 3 - 89 (Reapproved 1999). 1989. *Standard Practice for Conventions Applicable to Electrochemical Measurements in Corrosion Testing*. West Conshohocken, Pennsylvania: American Society for Testing and Materials. TIC: 247076.

ASTM G48-99a. 1999. *Standard Test Methods for Pitting and Crevice Corrosion Resistance of Stainless Steels and Related Alloys by Use of Ferric Chloride Solution*. West Conshohocken, Pennsylvania: American Society for Testing and Materials. Library Tracking Number-L1387.

ASTM G 5 - 94. *Standard Reference Test Method for Making Potentiostatic and Potentiodynamic Anodic Polarization Measurements*. Philadelphia, Pennsylvania: American Society for Testing and Materials. TIC: 231902.

ASTM G 61-86 (Reapproved 1998). 1987. *Standard Test Method for Conducting Cyclic Potentiodynamic Polarization Measurements for Localized Corrosion Susceptibility of Iron-, Nickel-, or Cobalt-Based Alloys*. West Conshohocken, Pennsylvania: American Society for Testing and Materials. TIC: 246716.

ASTM G1-81. 1987. *Standard Practice for Preparing, Cleaning, and Evaluating Corrosion Test Specimens*. Philadelphia, Pennsylvania: American Society for Testing and Materials. TIC: 246089.

ASTM G 1-90 (Reapproved 1999). 1990. *Standard Practice for Preparing, Cleaning, and Evaluating Corrosion Test Specimens*. West Conshohocken, Pennsylvania: American Society for Testing and Materials. TIC: 238771.

ASTM G5-87. 1989. *Standard Reference Test Method for Making Potentiostatic and Potentiodynamic Anodic Polarization Measurements*. Philadelphia, Pennsylvania: American Society for Testing and Materials. TIC: 246088.

NRC (U.S. Nuclear Regulatory Commission) 1999. *Issue Resolution Status Report Key Technical Issue: Radionuclide Transport*. Rev. 1. Washington, D.C.: U.S. Nuclear Regulatory Commission. ACC: MOL.19991214.0621.

QAP-2-0, Rev. 5, ICN 1. *Conduct of Activities*. Las Vegas, Nevada: CRWMS M&O. ACC: MOL.19991109.0221.

QAP-2-3, Rev. 10. *Classification of Permanent Items*. Las Vegas, Nevada: CRWMS M&O. ACC: MOL.19990316.0006.

UCRL-ID-132285. *Formulation and Make-Up of Simulated Dilute Water, Low Ionic Content Aqueous Solution*. Livermore, California: Lawrence Livermore National Laboratory. TIC: 245767.

UCRL-ID-132286. *Formulation and Make-Up of Simulated Concentrated Water(SCW), High Ionic Content Aqueous Solution*. Livermore, California: Lawrence Livermore National Laboratory. TIC: 245768.

UCRL-ID-132287. *Formulation and Make-Up of Simulated Acidic Concentrated Water (SAW), High Ionic Content Aqueous Solution*. Livermore, California: Lawrence Livermore National Laboratory. TIC: 245766.

YAP-SV.1Q, Rev 0, ICN 1. *Control of the Electronic Management of Data*. Las Vegas, Nevada: Yucca Mountain Site Characterization Project. ACC: MOL.19991008.0209.

8.3 SOURCE DATA

LL000201305924.120. General Corrosion and Localized Corrosion of the Drip Shield. Submittal date: 2/7/2000.

LL000201405924.121. General Corrosion and Localized Corrosion of the Drip Shield, (regression analysis). Submittal date: 2/7/2000.

LL981212005924.062. Degradation Mode Survey Candidate Titanium-Base Alloys for Yucca Mountain Project Waste Package Materials. Submittal date: 12/22/1998.